MIT Libraries | DSpace@MIT

MIT Open Access Articles

Lagoon of Venice ecosystem: Seasonal dynamics and environmental guidance with uncertainty analyses and error subspace data assimilation

Massachusetts Institute of Technology

Lagoon of Venice ecosystem: Seasonal dynamics and environmental guidance with uncertainty analyses and error subspace data assimilation

G. Cossarini,[1] P. F. J. Lermusiaux,[2] and C. Solidoro[1]

[1]   An ensemble data assimilation scheme, Error Subspace Statistical Estimation (ESSE), is utilized to investigate the seasonal ecosystem dynamics of the Lagoon of Venice and provide guidance on the monitoring and management of the Lagoon, combining a rich data set with a physical-biogeochemical numerical estuary-coastal model. Novel stochastic ecosystem modeling components are developed to represent prior uncertainties in the Lagoon dynamics model, measurement model, and boundary forcing by rivers, open-sea inlets, and industrial discharges. The formulation and parameters of these additive and multiplicative stochastic error models are optimized based on data-model forecast misfits. The sensitivity to initial and boundary conditions is quantified and analyzed. Half-decay characteristic times are estimated for key ecosystem variables, and their spatial and temporal variability are studied. General results of our uncertainty analyses are that boundary forcing and internal mixing have a significant control on the Lagoon dynamics and that data assimilation is needed to reduce prior uncertainties. The error models are used in the ESSE scheme for ensemble uncertainty predictions and data assimilation, and an optimal ensemble dimension is estimated. Overall, higher prior uncertainties are predicted in the central and northern regions of the Lagoon. On the basis of the dominant singular vectors of the ESSE ensemble, the two major northern rivers are the biggest sources of dissolved inorganic nitrogen (DIN) uncertainty in the Lagoon. Other boundary sources such as the southern rivers and industrial discharges can dominate uncertainty modes on certain months. For dissolved inorganic phosphorus (DIP) and phytoplankton, dominant modes are also linked to external boundaries, but internal dynamics effects are more significant than those for DIN. Our posterior estimates of the seasonal biogeochemical fields and of their uncertainties in 2001 cover the whole Lagoon. They provide the means to describe the ecosystem and guide local environmental policies. Specifically, our findings and results based on these fields include the temporal and spatial variability of nutrient and plankton gradients in the Lagoon; dynamical connections among ecosystem fields and their variability; strengths, gradients and mechanisms of the plankton blooms in late spring, summer, and fall; reductions of uncertainties by data assimilation and thus a quantification of data impacts and data needs; and, finally, an assessment of the water quality in the Lagoon in light of the local environmental legislation.

1.   Introduction

1.1.   Motivation

[2]   Traditional data-only coastal ocean monitoring programs give a limited description of a system, since they are made of a discrete, and usually low, number of stations, sampled at low frequency. For example, even in regions where important monitoring programs have been operating, and relatively "rich" data sets exist, typically, monthly snapshots of the coastal system are collected, but each snapshot is made of a small number of observation points [e.g., *Cloern and Dufford*, 2005; *Testa et al.*, 2008]. Traditional ways to extend the observations, punctual in time and space, to the whole monitoring region is through geostatistic methods, such as gridding, krigging or objective analysis [*Bretherton et al.*, 1976; *Chiles and Delfiner*,

[1]Department of Oceanography, Istituto Nazionale di Oceanografia e di Geofisica Sperimentale, Sgonico (TS), Italy.
[2]Department of Mechanical Engineering, Massachusetts Institute of Technology, Cambridge, Massachusetts, USA.

Figure 1. The Lagoon of Venice (Italy). The main nutrient discharge points are shown: rivers (arrows), islands of Venice and Murano, villages of Cavallino and Chioggia, and Industrial Area of P. Marghera. The Lagoon is connected to the Adriatic Sea through three inlets (Lido, Malamocco, and Chioggia). The 30 sampling points (labeled by B, shallow water sampling points) and C and M (channel sampling points) of the monitoring network MELa1 are also shown. Depths are in gray scale: darkest gray indicates a depth of 4 m and more.

1999]. However, such methods rely on assumptions which are not often satisfied in the coastal ocean.

[3] A step forward is to use data assimilation (DA) methods, which quantitatively combine ocean measurements and prognostic models in optimal ways to estimate the evolution of the fields and parameters of interest [*Bennett*, 1992; *Wunsch*, 1996; *Malanotte-Rizzoli*, 1996; *Robinson et al.*, 1998; *Robinson and Lermusiaux*, 2001; *Lermusiaux et al.*, 2006a]. DA enables the extrapolation in space and time of observations while using a priori information about the system dynamics. This a priori dynamics is summarized within prognostic models. Commonly, DA estimates are weighted averages of observed data and model predictions, in which the weights depend on prior uncertainties of the data and model. Our work is based on recent progress in biogeochemical-ecosystem DA (section 1.1). We implement a DA scheme, Error Subspace Statistical Estimation (ESSE) [*Lermusiaux and Robinson*, 1999; *Lermusiaux*, 1999a, 1999b, 2006, 2007; *Lermusiaux et al.*, 2002, 2006b], to investigate the seasonal evolution of nutrients, plankton, oxygen and lower trophic levels in the Lagoon of Venice, combining a rich data set with a physical-biogeochemical numerical model (section 2). To predict the largest uncer-

tainties, ESSE evolves an error subspace using a stochastic ensemble approach (Appendix B). The subspace is of variable size and spans and tracks the scales and processes where the dominant errors occur. When Lagoon data become available, they are assimilated in agreement with this error prediction. Presently, our ESSE estimates of seasonal biogeochemical-ecosystem fields, boundary forcing and their respective uncertainties lead to new descriptive and dynamics results in the Lagoon and allow us to provide quantitative guidance on local environmental policies.

[4] The Lagoon of Venice (Northern Adriatic Sea) is one of the largest lagoons in the Mediterranean Sea (about 390 km^2). Its average depth is of about 1 m, but its morphology is characterized by large shallow areas and by a network of deeper channels (Figure 1) including three narrow inlets that connect the lagoon to the Adriatic Sea, with a yearly averaged exchange of ca. 8000 m^3/s [*Gačić et al.*, 2005]. The Lagoon physics is driven by tidal and turbulent mixing [*Dejak et al.*, 1998] and is strongly influenced by external forcing from ocean inlets, river discharges and atmospheric forcing [*Lasserre and Marzollo*, 2000; *Solidoro et al.*, 2004; *Collavini et al.*, 2005]. Biologically, the Lagoon is a highly productive system, mainly dominated by spring and summer blooms of diatoms species [*Bandelj et al.*, 2008; *Facca et al.*, 2002]. Ecosystem seasonality is characterized by the increase of autotrophic community activity in late winter-spring, fuelled by inorganic nutrients delivered by river runoff and favorable light and temperature conditions. As the season proceeds, a multivorous food web develops with heterotrophic components and resuspended benthic diatoms. The ecosystem productivity reaches its maximum in summer when concentrations of dissolved inorganic nutrients are low and production is mainly sustained by recycling [*Bandelj et al.*, 2008]. In autumn, the productivity is limited by unfavorable light and temperature conditions and waters rich in inorganic nutrients form due to external inputs and accumulation after remineralization of organic material [*Solidoro et al.*, 2004]. High year to year variability is, however, observed [*Facca et al.*, 2002; *Solidoro et al.*, 2006] and annual ecosystem productivity is related to climate conditions [*Cossarini et al.*, 2008]. Seagrass and benthic macroalge, which were dominant during the early 1980s eutrophication period, are present now only in marginal areas [*Curiel et al.*, 2004]. Spatially, inner-outer and north-south gradients of nutrients and chlorophyll and plankton abundance diversity are usually observed [*Bandelj et al.*, 2008] due to the uneven distribution of nutrient loads from rivers and other discharge points along the lagoon edge [*Solidoro et al.*, 2004] and the complex hydrodynamics. Nitrogen and phosphorus loads are in the order of 4700 tN/a and 250 tP/a (see Appendix A for details).

[5] The Lagoon hosts important aquaculture and fisheries activities which depend on the quality and productivity of the system [*Suman et al.*, 2005]. A recent environmental legislation [*Ministero dell'Ambiente*, 1999] was introduced to protect the Lagoon and its environment. In particular, the legislation sets water quality targets for pollutants and nutrients concentrations and maximum permissible loads, underlining the need for an in depth knowledge of the spatial and temporal variability of the trophic state of the Lagoon and of the responses of the ecosystem to external pressures. This was one of the motivations for our field reconstruction via

ESSE which generates quantitative estimates of the Lagoon state and of its responses and improves upon standard data interpolation methods which do not account for ecosystem dynamics.

[6] In this study, new stochastic models for the biogeochemical-ecosystem dynamics of the Lagoon are developed and their parameters optimized. The sensitivity to initial and boundary conditions is quantified and half-decay characteristic times are estimated. We find that boundary forcing (rivers, open sea, etc) influence the Lagoon significantly and that modeling boundary uncertainties is necessary. Focusing on year 2001, we estimate the spatial and temporal variability of the trophic state of the Lagoon and of its response to external pressures, and provide guidance on monitoring and management. Findings include: quantitative characteristic times for phytoplankton and nutrients; relative importance of diverse natural and anthropogenic loads at the Lagoon boundaries and the variability of their impacts in the Lagoon's interior; dynamical connections among ecosystem fields and their variations in time and space; uncertainties of the field predictions and their monthly reductions by DA; and, an assessment of the water quality in the Lagoon in relation to local environmental legislation.

[7] In what follows, biogeochemical DA is overviewed (section 1.1). The data set, the coupled biogeochemical model and its prediction results are then described (section 2). Sensitivity analyses on initial conditions and boundary conditions are carried out and their results discussed (section 3). As a by-product, half-decay characteristic times are estimated for the Lagoon ecosystem dynamics. In section 4, the novel stochastic components of the ecosystem model and of its boundary conditions and the stochastic models of measurement uncertainties are determined. These prior error models are used in the ESSE scheme for uncertainty prediction and data assimilation, and an optimal ensemble dimension is estimated. The results of the assimilation are presented in section 5. The seasonal evolution of the: (1) principal eigenvectors of the state error covariance, (2) a posteriori fields and their dynamical interactions, and (3) prior uncertainty fields and their reduction by data assimilation, are described and studied. In section 6, the evolution of nutrient fields is discussed with respect to water quality targets introduced by the environmental legislation for the Lagoon. The conclusions and summary are given in section 7. The model characteristics are outlined in Appendix A, the prediction and assimilation components of ESSE in Appendix B and the objective analysis scheme in Appendix C.

1.2. Overview of Recent Biogeochemical-Ecosystem Ocean Data Assimilation

[8] Our research is based on progress made in the assimilation of biological data in coupled physical-ecosystem models, e.g., the report *Global Ocean Ecosystem Dynamics* (*GLOBEC*) [2000], comprehensive review by *Robinson and Lermusiaux* [2002] and special issue of *Gregoire et al.* [2003]. Such assimilation is feasible because of advances in biogeochemical-ecosystem ocean modeling as reviewed by *Hofmann and Lascara* [1998] and *Hofmann and Friedrichs* [2002]. New ocean observing platforms and sensors can now be utilized for biological-physical DA [*Dickey*, 2003].

[9] Since the early 2000s, DA for marine ecosystems has progressed, mainly in the use of more complete data sets

and more complex models, and in the application of more advanced DA schemes. Ensemble DA schemes and square root filters have been utilized in idealized 1D studies [e.g., *Eknes and Evensen*, 2002; *Raick et al.*, 2007]. More realistic data-assimilative ecosystem simulations with simplified Kalman filters [*Hoteit et al.*, 2004], quasi-local Kalman filters [*Hoteit et al.*, 2005] and singular evolutive interpolated Kalman filters [*Triantafyllou et al.*, 2003] have been successful in the Mediterranean. In semienclosed coastal bays such as Massachusetts Bay, real ocean data and coupled (sub)mesoscales physical-biogeochemical models have been combined using optimal interpolation [*Beşiktepe et al.*, 2003] and ensemble prediction schemes [*Lermusiaux*, 2006; *Lermusiaux et al.*, 2006a]. Physical DA for improved ecosystem dynamics continues to be investigated [e.g., *Berline et al.*, 2007] as well as DA with complete biogeochemical models but with simplified 1D physics [*Magri et al.*, 2005]. Since biological rates and parameters are not well known in the ocean, parameter estimation techniques are often applied for marine biological studies [e.g., *Solidoro et al.*, 2003; *Faugeras et al.*, 2004; *Losa et al.*, 2003, 2004; *Tjiputra et al.*, 2007].

[10] Intensive data-assimilative ecosystem studies have been carried out locally within focused biological sampling programs, e.g., in the central equatorial Pacific [e.g., *Friedrichs*, 2001, 2002] and western Atlantic [e.g., *Spitz et al.*, 2001]. Such results have lead to studies on the portability of marine biogeochemical models [*Friedrichs et al.*, 2007]. A related concept is that of allowing biological models to adapt and learn from the new data [*Lermusiaux et al.*, 2004; *Tian et al.*, 2004; *Lermusiaux*, 2007]. Because of availability of wide-coverage remote sensing data, surface ocean color data have been assimilated at regional, basin and global levels [*Garcia-Gorriz et al.*, 2003; *Hemmings et al.*, 2003; *Natvik and Evensen*, 2003; *Triantafyllou et al.*, 2007]. Global ecosystem modeling and geochemical DA for the Earth system are also investigated [e.g., *Ridgwell et al.*, 2007].

2. Data and Physical-Biogeochemical Model

2.1. Data

[11] The measurements utilized and assimilated in this study are part of experimental observations provided by the monitoring program MELa1, Monitoring of the Ecosystem of the Lagoon of Venice, promoted and managed by Consorzio Venezia Nuova on behalf of Venice Local Authority (Magistrato alle Acque). The program lasted for three years, from 2001 to 2003, and included almost monthly sampling campaigns in a network of 30 sampling points that cover the whole Lagoon (Figure 1). Two of the 30 stations, named M1 and M2 in Figure 1, are located just outside the Lagoon at the inlets of Lido and Chioggia. The other 28 stations are named C or B, distinguishing those located in channels from those located in shallow water areas. The sampling activities usually took about 8 hours in two consecutive days to cover the network of sampling points and were programmed to occur during neap tides to minimize the error due to nonsynopticity of the sampling [*Pastres et al.*, 2004; *Solidoro et al.*, 2004]. In this work we assimilate the data directly linked to the biogeochemical dynamics of the Lagoon: concentrations of Chlorophyll-a, dissolved inorganic nitrogen (DIN; sum
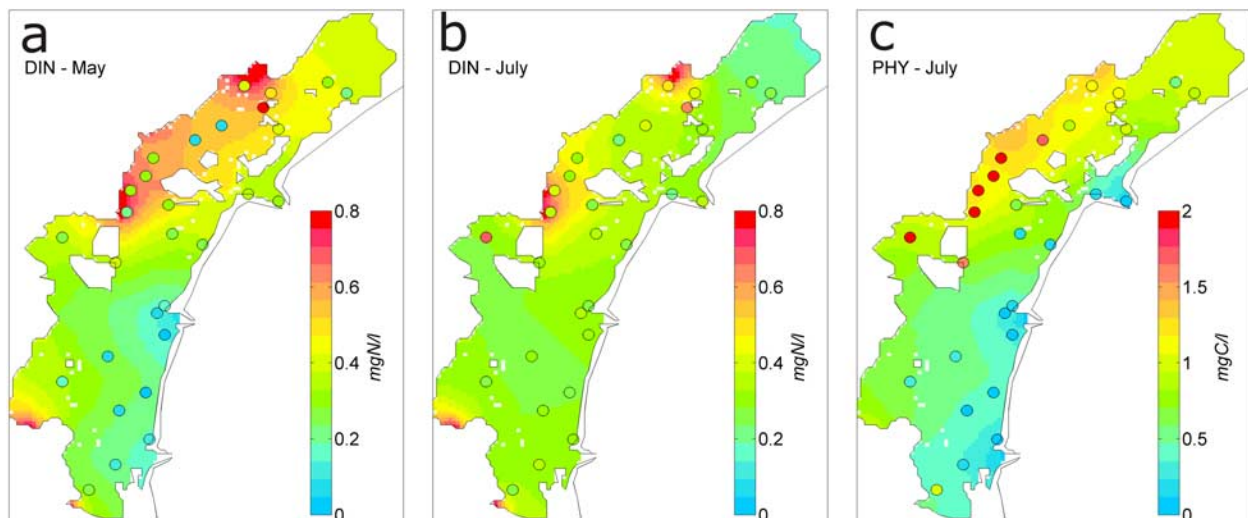
Figure 2. Model forecast of (a) May and (b) July 2001 for DIN and of (c) July 2001 for phytoplankton. Raw observation data are shown by the overlaid circles.

of ammonia and nitrate) and dissolved inorganic phosphorus (DIP). Chlorophyll-a values were determined according to the standard analytical procedure [*Istituto de Ricerca Sulle Acque* (*IRSA570.1Q59*), 1990], while spectrophotometric methods of *Strickland and Parsons* [1972] [*IRSA4010A-Q100*, 1994] were used to estimate nutrients concentrations. Before archiving and dissemination, data were checked for errors and anomalies, and quality certified [*Solidoro et al.*, 2004]. Chlorophyll data are transformed into carbon biomass data according to *Cloern et al.* [1995].

2.2. Coupled Physical-Biogeochemical Model

[12] The ecosystem of the Lagoon is simulated by coupled physical and biogeochemical models governing the evolution of 13 state variables in space and time. The formulation of this Trophic Diffusive Model (TDM) as well as its energetics, boundary conditions and comparisons to observations are given in Appendix A. Tidal effects over time scales larger than days are represented by a nonisotropic and nonhomogenous turbulent diffusion (Appendix A). The modeled set of biogeochemical state variables includes phytoplankton (PHY), zooplankton, nutrients (nitrate, ammonia and phosphorus), nutrient content in detritus and sediments, and dissolved oxygen (see Table A1 and Figure A1 in Appendix A). These variables can mimic essential features of the seasonal cycles of nitrogen and phosphorus, while limiting complexity. Since the water quality legislation focuses on nitrogen, our focus here is on DIN even though the model reproduces nitrate and ammonium dynamics separately as they affect oxygen dynamics in different processes. The biogeochemical model is forced by river inflows, meteorological fluxes and solar irradiance. For numerics, a finite difference scheme (Euler forward scheme for biogeochemical equations and 9 points Laasonen implicit scheme for transport equations) is used. The Lagoon is discretized into a regular grid of 300 m × 300 m in the horizontal (x, y) and a variable number of 1 m thick layers in the vertical (z). The integration time step is 1 hour, so that diel processes are resolved.

[13] The model, developed by a number of researchers working on the Lagoon of Venice in the last 15 years, has been utilized for several applications and process studies (see

Solidoro et al. [2005b] for a review). It has been calibrated and evaluated against different data sets and shown to be able to reproduce the timing and magnitude of the phytoplankton evolution and the spatial patterns and gradients of nutrients concentrations [*Pastres et al.*, 2005; *Solidoro et al.*, 2005a; *Cossarini et al.*, 2008]. Details on model formulation are summarized in Appendix A.

2.3. Model Hindcasts

[14] The coupled model hindcast estimate for DIN in the surface (0–1 m) layer (Figure 2a) illustrates the general spatial patterns of nutrients in the Lagoon at the end of one month (May 2001) simulation. Highest values of DIN are estimated to occur: (1) in the northern part of the Lagoon close to the Dese and Silone rivers; (2) in the central region which receives inputs from the industrial area of P.Marghera; and (3), near other significant rivers like Nav.Brenta and Lusore. Spotty high-nutrient-concentration areas are also simulated in the southern basin next to the southern tributaries. The lowest concentrations are near the Lagoon inlets, in response to exchanges with the Adriatic Sea that dilute nutrients in the Lagoon. While the general spatial patterns remain similar throughout the whole year in 2001, the strength of the gradients varies greatly as a function of the intensity of inputs and biological dynamics. For example, in July, due to the lower inputs and enhanced phytoplankton uptakes, the DIN concentrations decrease faster as the distance from the sources increases (Figure 2b). Phytoplankton, whose bloom is estimated to last from May to September, shows spatial pattern well correlated to those of nutrients as expected for estuarine systems [e.g., *Cloern*, 2001]. During July (Figure 2c), the highest levels of phytoplankton are estimated to occur in the region bounded offshore by Venice and Murano islands, and inshore by land where both nutrient concentrations and residence time are high.

[15] The model, which was calibrated for historical 1998 data [*Solidoro et al.*, 2005a] reproduces the main spatial patterns in the lagoon and is also able to capture several of the actual observation values (circles overlaid on the maps) in large parts of the lagoon. However, some discrepancies occur in specific areas, because of uncertainties in the model
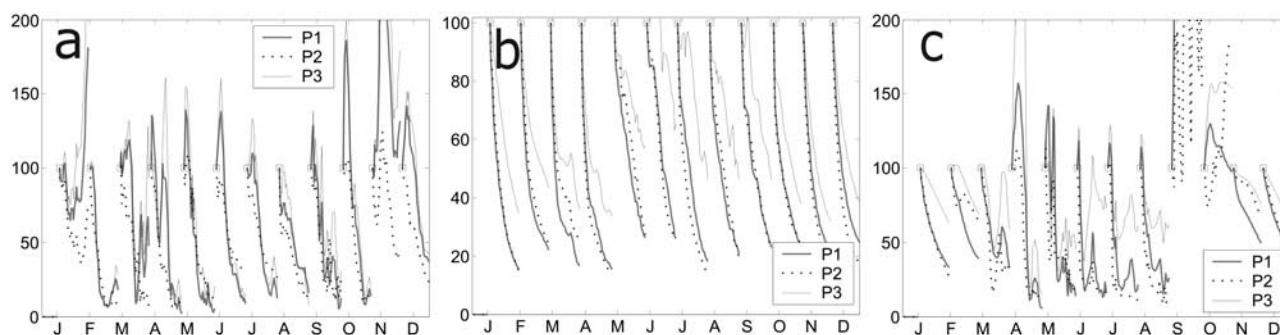
Figure 3. Evolution of the variance of the ensemble of runs for (a) phytoplankton, (b) DIN, and (c) DIP. For each month, the variance shown is a percentage relative to the variance of the latest analysis (on the first of the month, shown by open squares, this percentage is always 100). Each plot reports three curves, respectively, for three points of the Lagoon, namely the sampling points B01 (P1), B05 (P2), and B13 (P3).

formulation but more significantly due to errors in the prior estimates of the boundary conditions and forcing. For example, the region that receives inputs from the industrial area of P.Marghera shows the largest discrepancy (about 50%) between simulated and real DIN data for both months shown. Data assimilation is intended to solve these discrepancies. The goal is to obtain optimal estimates of nutrient and plankton fields for the entire Lagoon, correcting the initial and boundary conditions of the model as well as reducing effects of model uncertainties.

3. Sensitivity of the Ecosystem to Initial Conditions and Boundary Forcing Uncertainties

3.1. Initial and Boundary Prior Uncertainties

[16] There are several factors that affect the uncertainty in coastal predictions. The present ESSE methodology [*Lermusiaux*, 2006] aims to identify the dominant ones. The first factor is the initial uncertainty which is represented in ESSE by the sum of the dominant initial error covariance and of random errors. The other factors are: errors and simplifications in the model formulation itself and uncertainties in the model parameters and in the boundary conditions. These other factors contribute to errors during the time integration of the model. In general, the relative importance of the initial and of these other sources of uncertainties is a function of the duration of the prediction, of the internal dynamics and of the effects of boundary forcing.

[17] In the MELa1 monitoring program, the nutrient and phytoplankton data to be assimilated are measured over a 2 day period, once every month. Since this monthly data interval is not negligible when compared to the seasonal time scale, the relative importance of initial condition errors to that of during-the-integration errors is evaluated using sensitivity studies. Specifically, the questions are: by how much and for how long is the model output trajectory affected by the initial state of the system?, or as a corollary, when do the uncertain model dynamics, parameter and boundary forcing become predominant? The results are also useful to asses the expected impact of the assimilation of the monthly data in the Lagoon system.

[18] The sensitivity study is a numerical ensemble experiment. An ensemble of 100 initial conditions (ICs) is first

derived from a reference spin up solution to which white-in-space pseudorandom noise are added. This is done using

$$IC(x, y, z, \text{var})_j = IC(x, y, z, \text{var}) \cdot (1 + w_j) \quad \text{for } j = 1..100 \quad (1)$$

where the ICs are 3D fields of the initial state variables, w is a N(0,0.3) pseudorandom number [*Press et al.*, 1992]. Experimental data on daily variability (not shown) gave a mean coefficient of variation of 30% which is used as nondimensional noise standard deviation for the three state variables. These 100 runs are forced by the same driving functions and boundary conditions, and the evolution of the variance of the ensemble is computed for all model grid points. Twelve ensemble experiments are performed, one of each month. For each of them, the initial time is at the date of the MELa1 survey campaigns and the end time, the subsequent survey date. These monthly experiments allow investigating impacts of initialization uncertainties during different periods of the year, when different processes and driving forces are dominant.

[19] The evolution of the ensemble variances for three characteristic points (B01, B13 and B05 in Figure 1) are plotted in Figure 3, for phytoplankton, DIN and DIP. The three points are representative of a point close to the discharges of a river, to a Lagoon inlet and to the middle of the Lagoon basin, respectively. For each day, the ensemble variance plotted is relative to the variance at the starting time, in percentage. The 12 monthly sensitivity experiments are reported jointly, the vertical dotted lines indicate the start time of each ensemble run.

[20] From the plots in Figure 3b, the DIN variance decreased exponentially for all months and for each of the 3 points: after one month, the variance of the ensemble is about a fourth of its initial value. The same behavior is seen for DIP (Figure 3c), excepted for September, October and to a lesser extent also April, where the variance of the ensemble increases above the starting value before it decays. During these months and locally, in reduced mixing areas, the combination of low concentrations and active internal sources can lead to concentrations that become relatively much larger than their initial value (hence the peaks in Figure 3) even though in absolute terms they remain small.
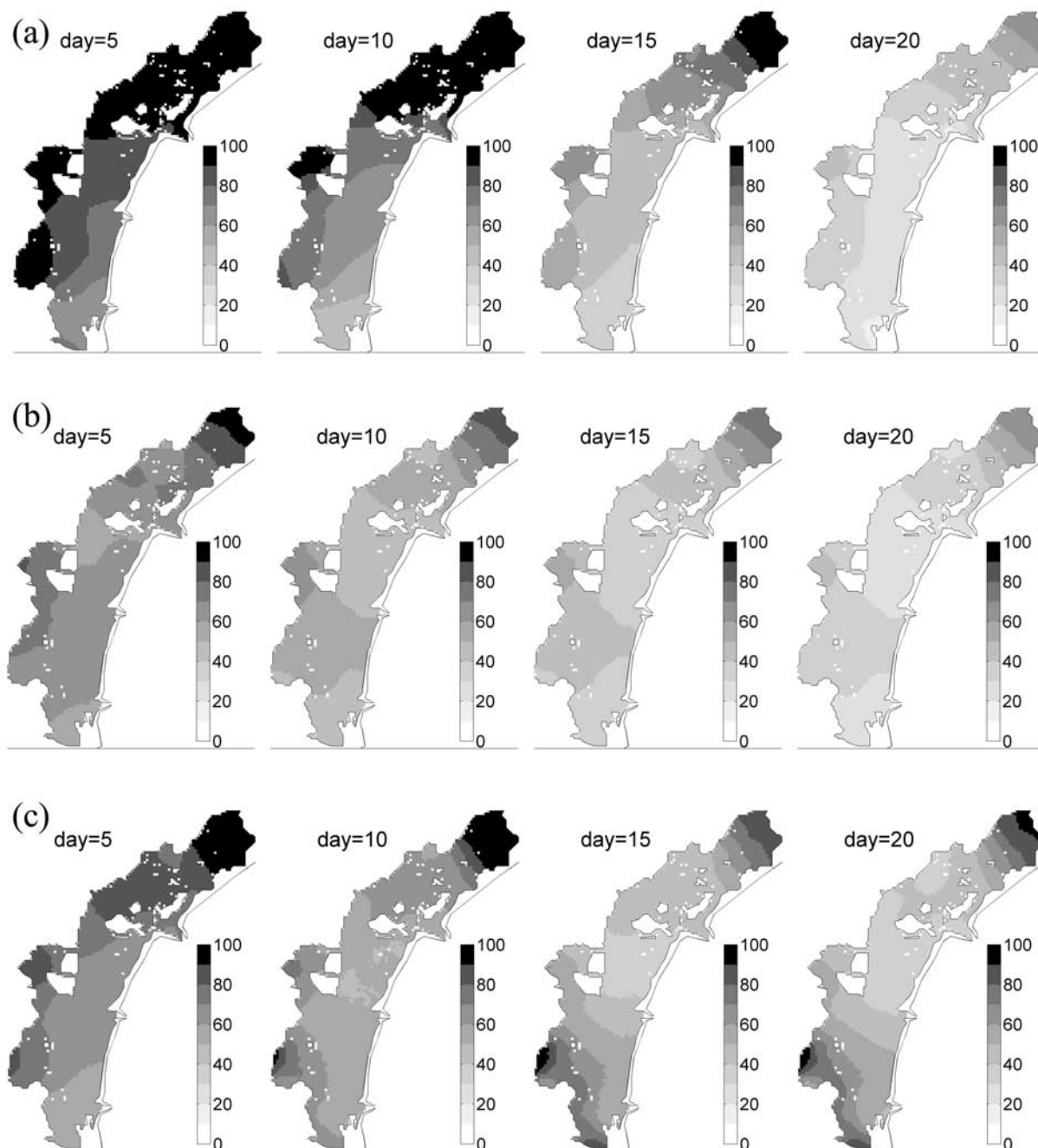
Figure 4. Spatial distribution of the relative ensemble variance for (a) phytoplankton, (b) DIN, and (c) DIP (percentages of the starting variance). The maps are refereed to the 5th, 10th, and 15th day after each analysis, and the values shown are averages of the 12 monthly maps.

[21] For phytoplankton (Figure 3a), the analysis can be separated among the biological active months, from April to September, and the other months (winter and fall) during which phytoplankton concentrations are small [*Solidoro et al.*, 2005a]. During the active months, phytoplankton variances increase in the first few days, and then mostly decrease exponentially, even though significant fluctuations occur. For the other months, the variance does not always decay, but concentrations are not significant.

[22] The evolution of the variance at the three points is similar but depends on the relative proximity to the bound-

aries. Spatial variability is investigated in Figure 4 which shows maps of the relative variance of the ensemble after 5, 10, 15 and 20 days since the start of each monthly ensemble simulations. For practicality, the variance is averaged over the 12 ensembles, leading to maps of the mean relative evolution for each variable. Effects of the boundaries (Lagoon inlets and discharge points) are clearly visible: they force the evolutions of the ensemble members to the fixed values of the BCs. In fact, the areas close to them are those where the variance decays the fastest while marginal areas, such as the marshes in the northern and southwestern regions, are less
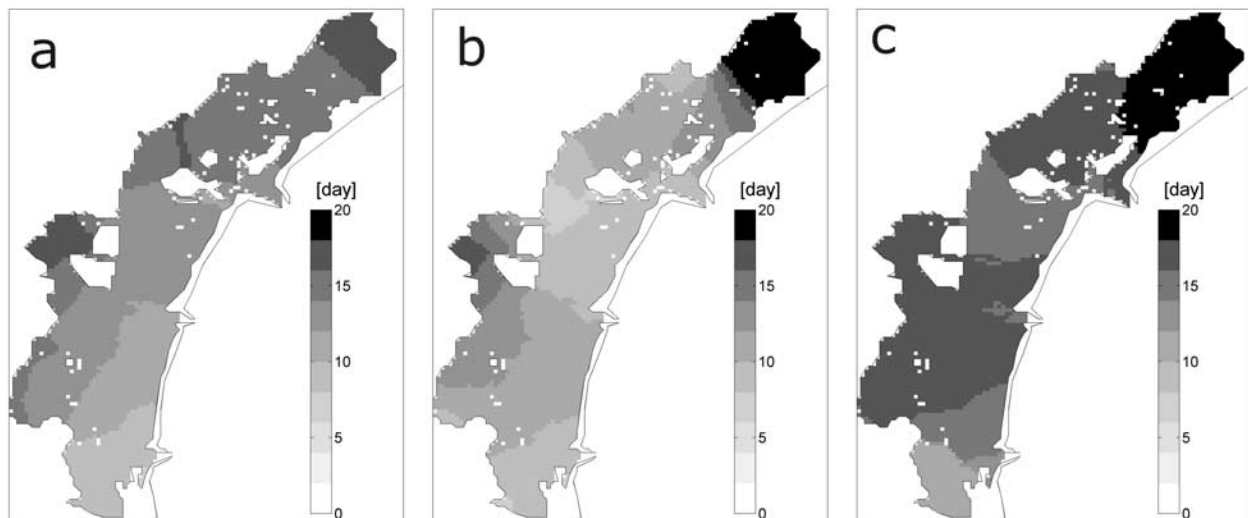
Figure 5. (a) PHY, (b) DIN, and (c) DIP. Maps of the time at which the variability of the ensemble is halved with respect to the starting value at the analysis time (first of each month). The values shown are averages of the 12 monthly maps.

affected by the constraint of the boundaries. Phytoplankton variance (Figure 4a) increases at the beginning of the run, because of the nonlinearity of growth processes, and afterward decreases as consequence of the dilution effects by the boundary constraints, starting from the Chioggia inlet and progressively from the other two inlets. Areas of low hydrodynamic energy, such as the northern basin and western part, sustain the highest variances in the maps. Note that if we consider only the April-to-September period when Phytoplankton is significant, the relative variance decrease is almost the same (about 10–15% faster). DIN is the variable that shows the quickest decay (Figure 4b): after just 10 days, the variance is half that of its initial value in most of the Lagoon. The inlets and major discharge points (Silone, Dese, Nov.Brenta and Nav.Brenta) decrease the initial variance and thus constrain the model forecast. The DIP variance maps (Figure 4c) are also constrained by boundaries, but in coastal areas in the southern basin, the DIP variance increase is large relatively, again due to low initial concentrations (as for September and October in Figure 3c).

[23] The results of the analysis suggest that the system on average forgets about 75% of the initial state variability after one month. Therefore, after one month of evolution, the system is significantly controlled by boundary conditions and internal dynamics, e.g., mixing. This is sensible since the Lagoon has a relatively high surface to volume ratio, almost 1/3 of the water volume is exchanged at each tide cycle, and the nutrient discharges from human and natural sources are dominant [*Zonta et al.*, 2005].

[24] Several DA schemes that forecast error covariances only perturb the initial state and propagate an ensemble of trajectories from the ensemble of initial states [*Eknes and Evensen*, 2002; *Natvik and Evensen*, 2003]. The conclusion of our sensitivity analysis applied to the Venice model is that stressors limit the influence of the initial state and its perturbations. Thus accurate models of the uncertainties that occur during the time integration [*Auclair et al.*, 2003; *Lermusiaux et al.*, 2006b] are also needed, especially for the boundary conditions (see section 4).

3.2. Half-Decay Characteristic Times

[25] It is of interest to quantify a time scale by which ICs are forgotten, i.e., the time by which the system trajectory is dominated by internal dynamics, driving forces and boundary conditions. This is done by computing the half-decay time, i.e., the time τ (day) by which the variance of the initial state ensemble is halved, at each grid point. Results are shown in Figure 5 for phytoplankton (Figure 5a), DIN (Figure 5b) and DIP (Figure 5c). For phytoplankton and DIN, inlets and rivers inputs were found to have a strong influence (Figure 4) and Figures 5a and 5b show that the half-decay time for these variables is less than 10 days in the central and southern Lagoon. For DIN (Figure 5b), it is also less than 8 days in a large zone of the northern subbasin close to the P.Marghera and to the rivers Silone and Dese. In that region, phytoplankton (Figure 5a) is less sensitive to river inputs (nutrient concentrations are quite high and no limiting effects are thus observed), consequently τ is around 14 days. Values of τ up to 16 days for DIN and phytoplankton are found in marginal areas of the Lagoon (northernmost and westernmost parts) which are characterized by very low eddy turbulence coefficients and by multiple islands. Averaging over the whole Lagoon, the mean τ is respectively 13 and 12 days for phytoplankton and DIN.

[26] For DIP, the mean value of τ is 17 days (Figure 5c): DIP in the Lagoon depends on its ICs for a longer duration than for the other two variables. This is because DIP is less sensitive to mixing processes and more sensitive to internal biogeochemical dynamics (as recycling, consumption, assimilation and releasing) than DIN. On average, τ for DIP is less than 12 days only in the areas close to the inlets and the P.Marghera and Nav.Brenta rivers. Excluding September and October from the analysis, the mean value of τ decreases to 15 days, confirming that these two months are characterized by processes of longer time scales.

[27] We find that our fields of coupled physics-biology half-decay times agree with physical residence times computed by *Zirino* [2005] and *Cucco and Umgiesser* [2006]. Many local ecosystem half-decay times are found smaller

than the 1-month interval between two consecutive MELa1 surveys. At those locations, after one month, initial conditions are less important than boundary conditions (open ocean, rivers and wind forcing) in driving the ecosystem dynamics. This is found for the whole lagoon, excepted for its northernmost region which is the furthest from lateral boundaries and where internal nonlinear biological dynamics are strong. Since boundary conditions are not well known, after one month the variance of the model solution due to boundary uncertainties could be significant. Boundary uncertainties have to be accounted for to obtain a proper forecast of total error statistics. The covariances of these total uncertainties are the main input to the assimilation step (Appendix B). They must be accurate enough to allow the survey data to correct the model solution and its parameters adequately.

4. Novel Stochastic Ecosystem Model, Boundary Forcing, and Measurement Model

[28] Our modeling includes the Lagoon-specific stochastic models that represent the dominant prior uncertainties in the physical/biogeochemical model of the Lagoon and its external forcing. This novel stochastic formulation of the ecosystem model including stochastic boundary conditions is presented and discussed next (section 4.1). These uncertainty models are then utilized in a sensitivity analysis on the dimension of the ensemble of forecasts required for sufficiently accurate error covariance estimates (section 4.2). Finally, the results of the formulation and tuning of the measurement uncertainties are summarized (section 4.3).

4.1. Stochastic Formulation of the Ecosystem Model and Boundary Forcing

[29] Each member of the ensemble is now generated by integrating a new stochastic model. The stochastic differential equations are obtained by forcing the deterministic TDM model and its boundary conditions (Appendix A1) with random noise components that represent the expected statistics of these model and boundary errors.

$$dC_i = M(C, t) + d\eta_i \qquad (2)$$

$$C_i(t = 0) = C_0 \qquad (3)$$

$$C_i|_{x=inlet} = C + \varepsilon_i \qquad (4)$$

$$C_i|_{x=river} = \Phi_C + \upsilon_i \qquad (5)$$

where η, ν and ε are general colored error noises added to model and boundary conditions whose probability distribution is fitted in this section. For the TDM model, an internal model random noise is added at each time step and each grid point of the model domain. This error model accounts for the uncertainty in model equations and prior parameters (kept fixed at the values used by *Solidoro et al.* [2005a]). The boundary conditions are the inputs of nutrients from the river and urban discharges (equation (5)) and the exchange fluxes at the Lagoon-Adriatic Sea inlets (equation (4)). For

the exchanges at the Lagoon-Adriatic Sea boundaries (three inlets), a random noise (ε) is added to the reference daily evolution of concentrations of nutrients, phytoplankton and zooplankton (Appendix A4 describes the formulation of this boundary condition and computation of the reference evolution). Then, a random error (υ) is added to each reference evolution of the daily discharges (Φ_c) of nitrogen and phosphorus at the rivers or urban discharge points. The daily discharges are computed from monthly or annual data (Appendix A4 and Table A2), using a formulation that depends on the daily rain and typology of the source (see Appendix A4 for details).

[30] The formulation of prior error models is a critical step in the assimilation scheme. For example, if the data uncertainties are small enough, the statistics of the predicted total uncertainty should be comparable to those of the model-observation misfits. In general, forecast errors and observed errors should be compatible. To tune the model and boundary uncertainty parameters, test simulations were carried out. Two factors were found to be most important: the standard deviation (amplitude) of the random noise and their temporal and spatial correlation. Findings are reported based on a subset (Table 1) of these tests.

[31] The first two simulation cases (named M30 and M60) are forced by independent white random noise. Random forcing is added to the model equations (DIN, DIP, phytoplankton, zooplankton and detritus fields) at each time step and each grid point of the domain, with normal distribution of zero mean and normalized standard deviations equal to 5% for M30 and 10% for M60. At each boundary (i.e., inlets and nutrient discharges), white random noise is also added at each time step, with standard deviation equal to 30% for the M30 case and 60% for M60. In the next two test cases (M30A and M60A), the error model for the dynamical TDM is that of the M30 and M60 settings, but the boundary error model is different. The random error noise at the boundaries is assumed to be correlated in time. In practice, for each state variable and each boundary location, a single perturbation is added to the whole evolution of the boundary. Finally, the last two representative test cases, M30B and M60B, differ from M30A and M60A because the random noise added to the model fields is correlated in space, taking the form of a random patchy field. To obtain such a field, a number of points $(30-50$ points) of the domain are randomly chosen using uniform probability at each time step. A patchy error noise is then added in the surrounding (see Table 1, M30B and M60B under Internal Modem Error, where dist is the distance between one of the chosen points and its surrounding (x, y), and d_0 is a decay distance in the horizontal, set to 1 km). The random noise on boundaries is as in M30A and M60A.

[32] To limit computational costs (an ensemble of 300 runs of 30 days long lasts about 17 h on a Linux AMD opteron64 (2.0 GhZ) workstation), simulation tests were performed for a single month. The month of June was chosen because it is representative of conditions observed for part of the year. The June nutrient fields show significant gradients due to important late-spring input and the phytoplankton field is characterized by the condition of an already started bloom. For each case, an ensemble of 300 simulations is run from May to the MELa sampling date of June. The May ICs, common to all tests, are a spin off solution from the reference hindcast. At

Table 1. Definition of Representative Test Cases for the Tuning of Model and Boundary Errors

	Internal Model Errors			Boundary Condition Errors		
	St_M (%)		Stochastic Forcing Properties	St_{BC} (%)		Stochastic Forcing Properties
M30	5	$\eta_{l_i} \in N(0, st_M)$	Random at each time step and grid point	30	$\varepsilon_i, \nu_i \in N(0, st_{BC})$	Random at each time step and each boundary location
M60	10	$\eta_{l_i} \in N(0, st_M)$	Random at each time step and grid point	60	$\varepsilon_i, \nu_i \in N(0, st_{BC})$	Random at each time step and each boundary location
M30A	5	$\eta_{l_i} \in N(0, st_M)$	Random at each time step and grid point	30	$\varepsilon_i, \nu_i \in N(0, st_{BC})$ fixed over 1 month	Random at each boundary location but constant over one month
M60A	10	$\eta_{l_i} \in N(0, st_M)$	Random at each time step and grid point	60	$\varepsilon_i, \nu_i \in N(0, st_{BC})$ fixed over 1 month	Random at each boundary location but constant over one month
M30B	5	$\eta_{l_i}(x,y) = \eta_{l,0} \cdot 10^{-dist/d_0}\eta_{l_i,0} \in N(0, st_M)$	Patchy perturbations on the model domain	30	$\varepsilon_i, \nu_i \in N(0, st_{BC})$ fixed over 1 month	Random at each boundary location but constant over one month
M60B	10	$\eta_{l_i}(x,y) = \eta_{l,0} \cdot 10^{-dist/d_0}\eta_{l_i,0} \in N(0, st_M)$	Patchy perturbations on the model domain	60	$\varepsilon_i, \nu_i \in N(0, st_{BC})$ fixed over 1 month	Random at each boundary location but constant over one month

the date of the MELa sampling, for each test, we compute the standard deviation of the ensemble of runs and the misfit between the observations and the mean of the ensemble. Results are discussed next.

[33] First, we compare in Figure 6 the median of the model-observation misfit distribution for the 30 MELa1 points (horizontal dashed line in Figure 6) with the distribution of the standard deviation values of the six representative cases (box plots in Figure 6). For each of the 30 MELa points, the misfit is the absolute difference between the values of observations and the mean of the 300 runs of each ensemble for PHY, DIN and DIP. Similarly, for each of the 30 data locations, the standard deviation of the 300 runs is computed and the distribution among the 30 points is described by the box plots. The first two cases, M30 and M60, have a model uncertainty too low when compared to the model-observation misfit. This is because the noise added to the model fields is uncorrelated in space: they are quickly smoothed and dissipated by diffusion transport processes, both in the interior and near boundaries. A significant increase in uncertainty is obtained by the "A" setting. Introducing a temporal correlation on the boundary random noise causes a larger dispersion of runs within ensembles. Between the two "A" settings, M60A allows for a substantial increment of the forecast error: it appears satisfactory for DIN, but it is still not enough for PHY and DIP. The use of patchy random perturbations in the B settings improves the PHY fit (PHY is often observed to have a patchy variability). Comparing M30B to M60B, the choice of st_M and std_{BC} equal to 10% and 60% (M60B) gives the better compatibility between the data-model misfits and the model and boundary error models, for all three variables.

[34] When compared to the A cases (noise with no correlations in space), the patchy perturbation of the B cases causes larger local divergence of solutions within short times. Any two simulations in the B ensembles can thus differ significantly, especially where the eddy diffusivities are small in the Lagoon. This effect is more evident in the phytoplankton fields than in nutrients since the spatial dynamics of DIP and DIN are affected more by the uncertainties added to the discharges.

[35] Secondly, the set of maps in Figure 7 compares the standard deviations of the ESSE predictions of forecast errors of DIN for the six error cases of Table 1. The misfits at the 30 MELa data points (solid dots) are also overlaid on each of the standard deviation maps, to allow direct evaluations. The central area and the area north of Venice (Figure 7) show the highest model-observation misfit. These areas are critical for our uncertainty model (also true for other variables, not shown). In fact, they exhibit the highest observed variabilities [*Solidoro et al.*, 2004]. This is because they are influenced by the strongest input sources with their own intrinsic variability, and because they are characterized by low bathymetry and high residence times [*Solidoro et al.*, 2004; *Cucco and Umgiesser*, 2006]. As a result, the variability of the internal biological dynamics is important and the absolute data-model misfit is the largest in these areas (note that relative data-model misfits normalized by the local variability are more uniform in space). Comparing the maps of the different test cases confirms that the M60B setting leads to model-predicted error statistics most compatible with the data-
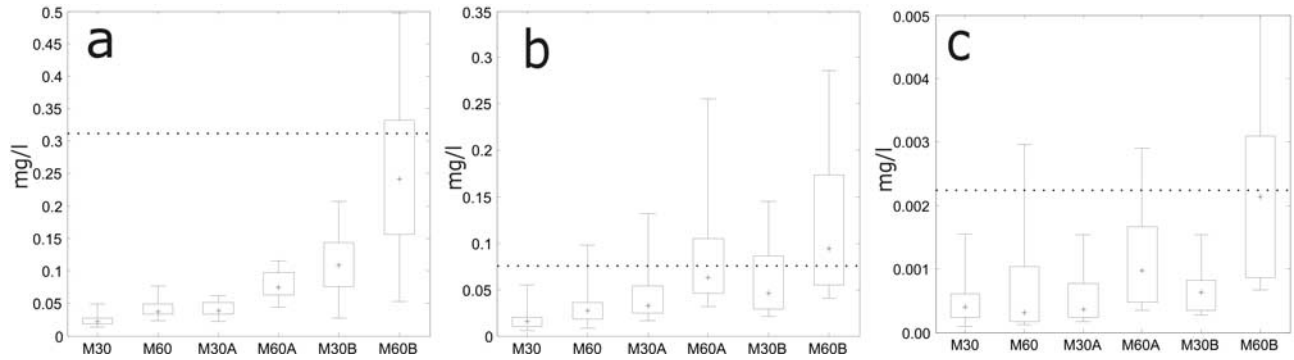
Figure 6. Median of the model-observation misfit for the 30 MELa points (dashed line) and distribution of the model prediction of the error in (a) PHY, (b) DIN, and (c) DIP for the six experiments. The box plots report the median, interquartile range (IRQ), and min-max range of the distribution of the standard deviation of the six ensemble tests.

model misfits. They do not match well only in very few marginal areas close to discharge point sources (e.g., like in P.Marghera) whose discharges are poorly known.

[36] In conclusion, the case M60B is chosen as best error model. For verification, it is run for each of the 12 monthly assimilation periods. For each month, an ensemble of 300 simulations is run for one month, from one sampling date to the next. At the time of assimilation events we again compare the model-data misfit (distance between tick black line and stars in Figure 8), and the model forecast error (length of the vertical bars in Figure 8). The requirement of strict compatibility between predicted error and data-model misfit is fulfilled for all variables, but for PHY in August and September, and DIP in May, November and December, and to a less extent in April. This condition is sufficient since for these months, some ensemble members in M60B have very small data-model misfits.

4.2. Ensemble Size Requirements

[37] Before the assimilation studies, sensitivity analyses were carried out to determine the mean size of the ensemble for which the error covariance estimate converges. To do so, we use the similarity coefficient $\rho = \dfrac{\sum_{i=1}^{\min(\tilde{p},p)} \sigma_i\left(\Pi^{1/2} E^T \tilde{E}\tilde{\Pi}^{1/2}\right)}{\sum_{i=1}^{\min(\tilde{p},p)} \sigma_i(\tilde{\Pi})}$,

see *Lermusiaux* [1999b] and Appendix B for definitions. This coefficient assesses when new members in the ensemble do not significantly change the dominant eigendecomposition of the error covariance. It was found that when ρ is larger than about 95–98%, the variance and structure of new forecast members can be well explained by the eigenvectors and eigenvalues of the previous ensemble. Results are reported in Figure 9, where the ticks of the x axis denote the size of the previous and current error subspace estimates (see numbers in square brackets beside the plot markers). The chosen criterion limit of 97% is depicted by the horizontal dotted line. Convergence of the error subspace is estimated to occur with 180 runs for DIN for all of the monthly simulations and with 220 runs for DIP and phytoplankton. These last two variables have spatial dynamics more complex than that of DIN and a larger number of runs is required to constrain the error subspace. Further, a slight time variation in the behavior of the similarity coefficient is noticed for

phytoplankton. In fact, spring bloom months (March, May and June) converge more slowly than for other seasons, which is due to the active dynamics during this period. No temporal pattern is clear for the DIN and DIP similarity coefficients. In conclusion, since there are no real-time constraints, a common large dimension of the ensemble is utilized for all monthly experiments and for all variables: the assimilation studies are performed using an ensemble of 220 runs.

### 4.3. Stochastic Formulation of the Measurement Model

[38] A stochastic measurement model is not trivial since its error models account for several sources of uncertainties, including: sensor errors, errors $\mathbf{y}° - H(\hat{\mathbf{x}}(-))$ in the measurement model itself (e.g., due to variables conversions), and errors of representativeness (e.g., inadequacies of the sampling for the processes studied). In our model, standard error deviations are modeled as the sum of additive and multiplicative errors. Specifically, inserting all observations into a vector $\mathbf{y}°$, the error standard deviation of each measurement is defined as

$$\varepsilon_{obs} = \mathbf{c}_{obs} + \alpha\mathbf{y}° \qquad (6)$$

where: $\mathbf{c}_{obs}$ is a background data error vector of elements set to 0.025, 0.025 and 0.005 mg/l for phytoplankton, DIN and DIP, respectively; and, α is a scalar coefficient that multiplies the data value for modeling proportional data errors. As a whole, the vector ε_{obs} in (7) is the diagonal of the measurement error covariance matrix $\mathbf{R}$ (see Appendix B2). The off-diagonal elements of $\mathbf{R}$ are here assumed null.

[39] In many applications, data error is set based on experience; only a few studies investigated effects of the data error on the DA results [e.g., *Natvik and Evensen*, 2003]. Here, we tested different values of $\mathbf{c}_{obs}$ and α for each observation type and evaluated their effects on a posteriori fields. Data assimilation tests with α set to 0%, 1%, 5%, 10%, 20% and 50% were carried out for each month (plots not shown). The results are that for α at 50% or higher, corrections are too small, and that for α at 1% or smaller, they are too strong and too localized. The magnitude of the state correction (posterior innovation vector) was then compared to the forecast error for the M60B case (section 4.1). This comparison was done for each month, for a set of values for
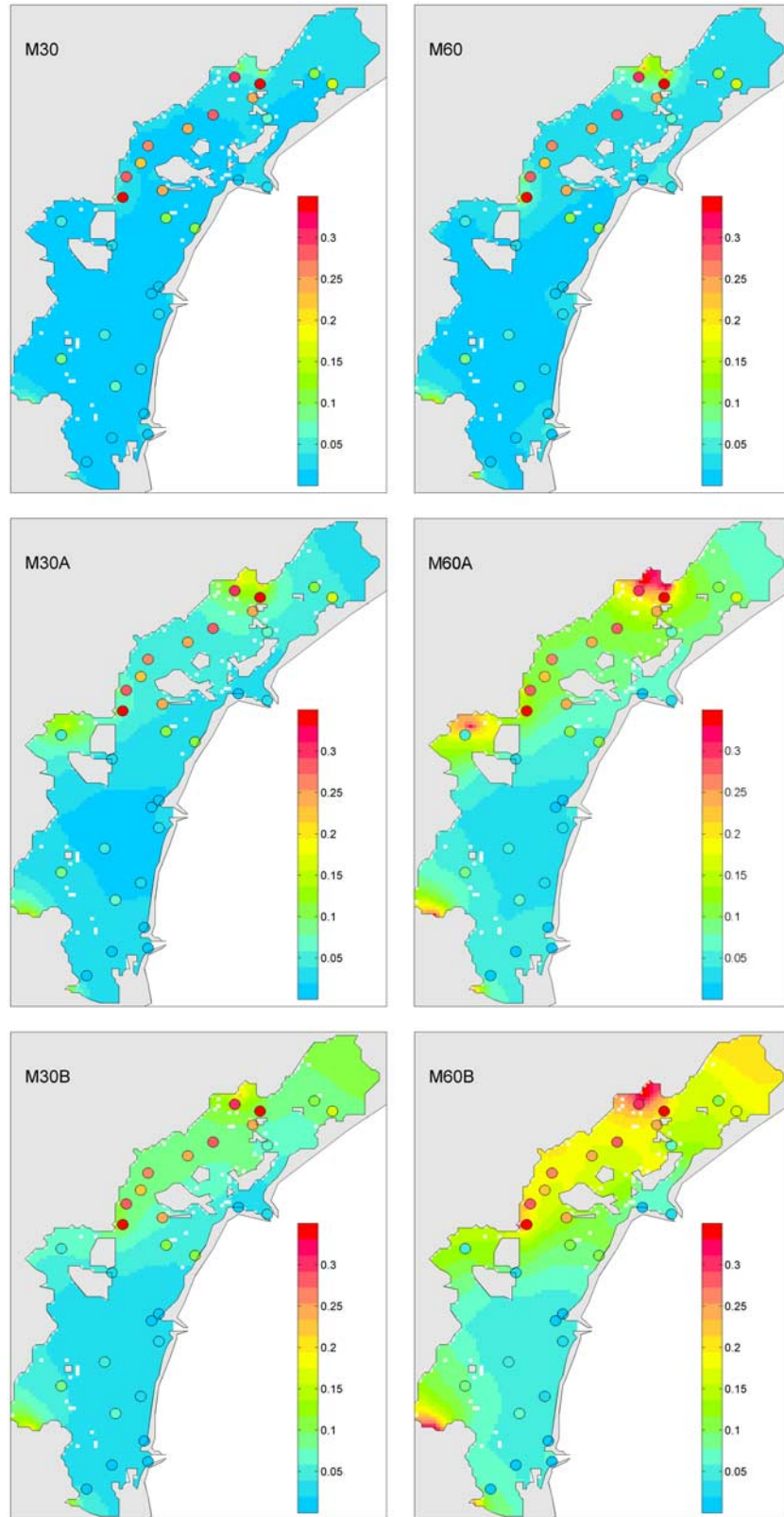
Figure 7. Maps of the ESSE predictions of the forecast error (standard deviation of the ensemble), overlaid with the misfits (colored solid dots) between the model predictions and the observations at the 30 MELa points, for DIN (mg/l) for the six experiments listed in Table 1. Dots and maps use the same color scale.
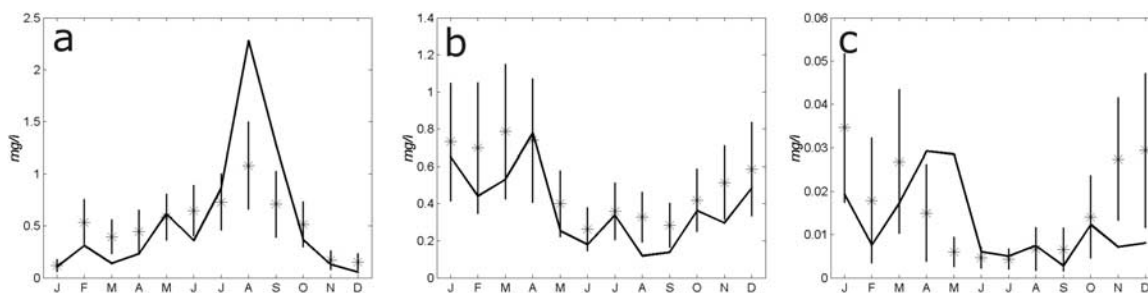
Figure 8. Comparison between monthly mean evolution of observations (thick black line) and monthly mean model evolutions (asterisks) for (a) PHY, (b) DIN, and (c) DIP. Vertical lines show the mean model forecast errors for the M60B setting. Model means are computed at the data points only.

α and c_{obs}. In order to filter the data noise and errors of representativeness (e.g., data points that are close but with significantly different data values), a value of $\alpha = 10\%$ and the above mentioned values of c_{obs} were selected.

## 5. Ecosystem Fields, Dominant Uncertainty Decomposition, and Their Seasonal Dynamics

[40] The main results of the 12 assimilation experiments (one for each of the monthly MELa1 surveys) are presented next. ESSE provides an optimal estimate of the state variable fields and covariances (Appendix B) and thus allows the investigation of the ecosystem dynamics. The results of the dominant decompositions of covariance matrices are first shown in section 5.1. These dominant eigenvectors describe the scales and patterns where dominant uncertain variability occurs in the system, e.g., the most energetic spatial patterns of the lagoon ecosystem. In section 5.2, the posterior ecosystem fields, i.e., the optimal combination of the observations with model fields, are presented and discussed. In section 5.3, the uncertainty estimates for these fields and their reduction by data assimilation are examined. Our study of the seasonal evolution of the dominant modes of variability (eigenvectors) and of the posterior ecosystem fields and

their uncertainties leads to new quantitative understanding of the seasonal evolution of the trophic state of the system.

5.1. Seasonal Evolution of Ecosystem ESSE Eigenvectors and Their Comparisons to Data

[41] The 12 first eigenvectors of DIN, one for each of the monthly assimilation events, (Figure 10a) explain more than 30% of the total variance of DIN in all months. The explained variance is the largest during late winter and spring months (39.8% in June) and minimum in summer (29.0% in July) when the variability is spanned in a higher number of eigenvectors and field gradients are less pronounced (see section 5.2). The first eigenvectors describe a typical spatial pattern that is associated with the influence of the discharges from the Dese and Silone rivers, in all months. These two rivers accounts for more than 40% of the annual runoff of the drainage basin [*Zuliani et al.*, 2005] and, since they are natural systems, they are sensitive to effects of meteoclimatic variability [*Zonta et al.*, 2005]. As a result, their uncertain variability has a great influence in the dynamics and variability of a large part of the northern basin of the lagoon.

[42] The second eigenvectors (Figure 10b) account for from 12% (in January) to 23% (in December) of the total variance. They are associated to different areas according to
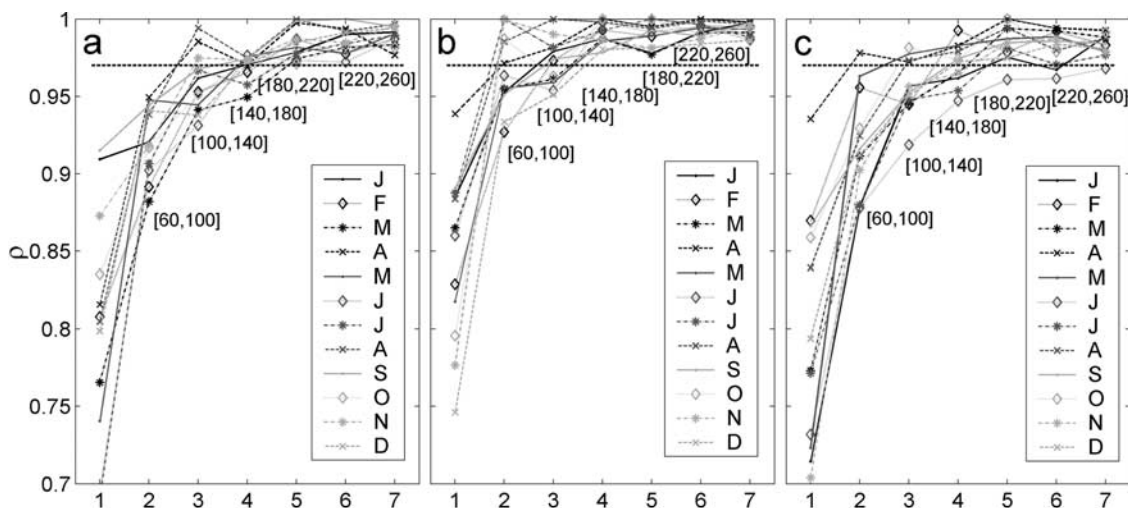
Figure 9. Evolution of the similarity coefficient ρ for (a) phytoplankton, (b) DIN, and (c) DIP as a function of the size of the ensemble. Twelve plots, one of each month, are reported together with the criterion limit of 97% (horizontal dotted line). The pairs beside the markers denote the respective size of the previous and new estimates.
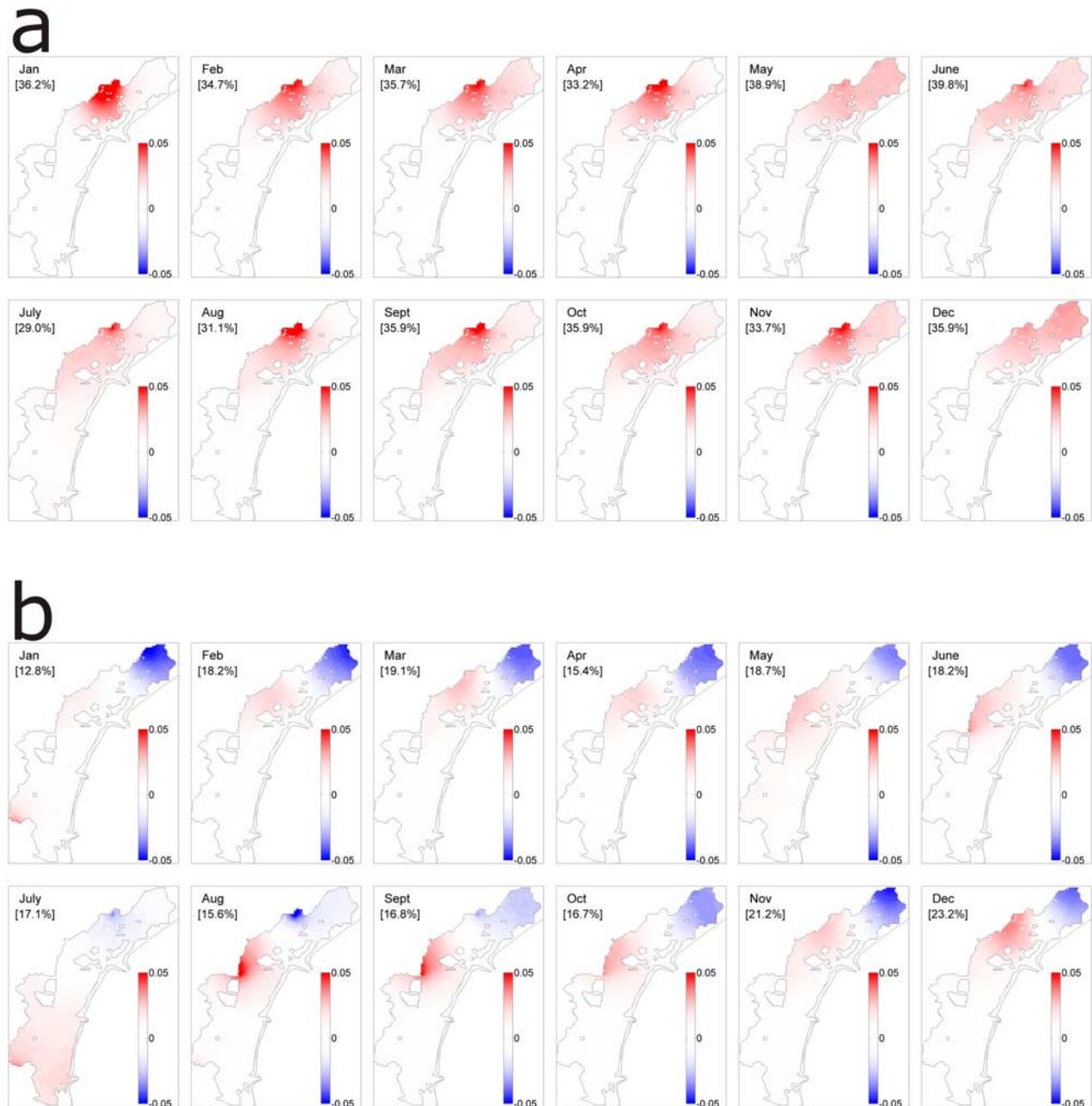
Figure 10. Maps of the (a) first and (b) second eigenvector for each monthly assimilation event for DIN. The variance explained by the eigenvector is reported in square brackets.

local dominant processes at the different months. A common feature to most second eigenvectors is that the northernmost part of the lagoon (blue area in the maps) is either decoupled from or in opposition with the local sources of nutrient. In fact, nutrient discharges from the rivers Dese and Silone are mainly driven toward the south by the net effect of channels that converge into the Lido inlets, leaving the northernmost part relatively isolated from the variability of those rivers. Other features of the second eigenvectors identify areas characterized by high uncertainty located near the discharge points of other rivers different than the two biggest ones. The

importance of the discharges from the industrial area of Porto Marghera and Nav.Brenta is shown in the maps of May, June, August, September and October. The maps of January and July highlight the relevance of the discharges from the rivers located in the southern part of the lagoon, while effects of northern rivers other than Dese and Silone are depicted in the remaining maps.

[43] An Empirical Orthogonal Function (EOF) analysis has been applied to DIN data of 2001. It shows that the most energetic spatial patterns can be described by the first three eigenvectors (Figure 11) that account together for more than
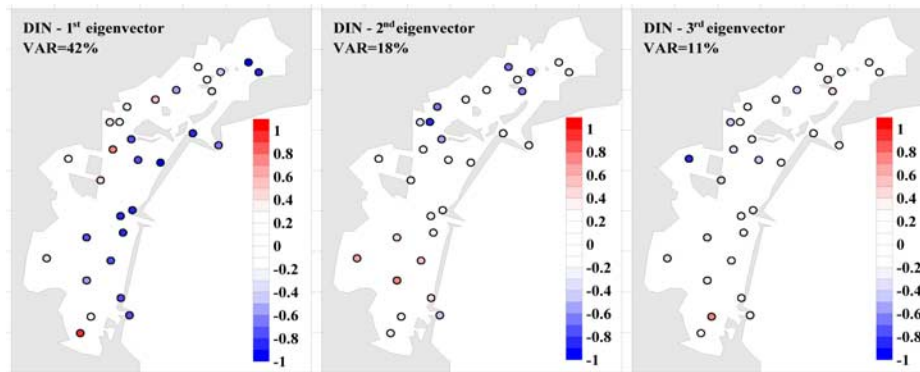
Figure 11. First 3 eigenvectors of an EOF analysis on DIN concentration. Data were detrended. The first 3 eigenvectors explain 71% of the variance of the data of 2001.

of the 70% of the total variance, indicative of a red spectrum in space. The areas close to the rivers and inlets are those characterized by the highest variability. In particular, the patterns shown by eigenvectors identify the areas linked to the stations located in the central and southern part of the Lagoon close to Malamocco and Chioggia inlets (1st eigenvector, which correspond to the mean gradient). The variability from this mean gradient corresponds to stations near the Dese and Silone rivers (2nd eigenvector) and to stations located close to the industrial area of P.Marghera (2nd and 3rd eigenvectors). This agrees with the ESSE results which identify dominant variability from the mean gradient and importantly cover model points everywhere (including near rivers not sampled in the MELa network in 2001). It is worth noting that the EOFs also show that the northernmost part of the Lagoon is essentially decoupled from the patterns linked to the northern rivers. The results of the ESSE and EOFs analyses on DIP and phytoplankton (not shown) confirm that most of the variance of the system is linked to impacts of external boundaries (inlets, two rivers Dese and Silone, and industrial area of P.Marghera). However, for DIP and phytoplankton (only for the active months), internal dynamics is found to be more significant in the dominant ESSE uncertainty modes and data EOFs than for DIN.

5.2. Seasonal Evolution of Ecosystem Fields

[44] The results of the DA sequence analysis are showed in Figures 12, 13 and 14, reporting the ESSE maps of the "a posteriori" fields for phytoplankton, DIN and DIP, respectively. Each map shows also the observations (overlaid colored circles) used to correct the "a priori" model predictions. Since the dynamics and observations have been quantitatively integrated by the ESSE assimilation scheme, the sequence of maps allows an optimal study of the evolution of the trophic state of the ecosystem across the Lagoon and its seasons. The measured values at data points and the posterior fields compare well (in part because all errors were tuned, see sections 3 and 4), but importantly, the field estimates cover the whole basin which allow dynamical studies.

5.2.1. Phytoplankton Biomass

[45] The seasonal evolution of phytoplankton (Figure 12) is forced by the annual cycles of temperature and light availability. The sequence of maps shows very low concentration during fall and winter and a bloom that starts in May and lasts until September. As light and temperature condi-

tions become favorable (in May 2001), the bloom is driven by the availability of nutrients discharged by rivers: we computed a significant correlation between spring maps of phytoplankton concentration and DIN (0.788 and 0.853 in May and June respectively). The spring bloom is found to start in the central-northern Lagoon and to persist there for the first 2 months (May/June) with concentrations up to 1 mg/l. Then, it spreads over the entire Lagoon during July when it reaches values up to 2 mg/l in the northern region and when the mean concentration in the Lagoon increases to value above 0.7 mg/l. The annual maximum concentrations are observed in August when the bloom covers almost the whole Lagoon with concentrations between 1.2 mg/l in the central Lagoon up to 2.0–2.5 mg/l in the northern Lagoon.

[46] The largest correction in the assimilation was produced for the August map which showed an average a priori model-observation misfit of about 1.1 mg/l. Several areas of the lagoon were increased, producing a mean correction of about 0.8 mg/l. This high a priori misfit is in part due to uncertainties in river and industrial forcing estimates which were corrected by ESSE. It is also due to an underestimation of the maximum growth rate for phytoplankton: this rate was calibrated based on 1998 data [*Solidoro et al.*, 2005a]. This outlines the feasibility of using a DA method for the estimation of the system state, even with imperfect parameters; ideally, a continuous recalibration [*Lermusiaux*, 2007] of the model could be implemented.

[47] The very low concentration of DIN (both predicted and observed) in August (see Figure 13) suggests the high capability of the ecosystem, through rapid regeneration processes, to sustain the phytoplankton bloom up to the observed levels. In September, the bloom begins to decrease, and after October the productivity of the system is limited by light availability and temperature level. It is worth noting that in February the assimilation scheme corrects the model forecast for a medium-amplitude bloom in the southern Lagoon (larger concentrations, but not above 0.6 mg/l). Such winter blooms can be due to different species than those that dominate during spring and summer seasons [*Facca et al.*, 2002]. Since no nutrient limitation is detectable, the assimilation can successfully incorporate local winter blooms to model predictions, even when the model has been calibrated to follow the evolution of a phytoplankton specimen pool characterized by a somewhat different light and temperature adaptation.
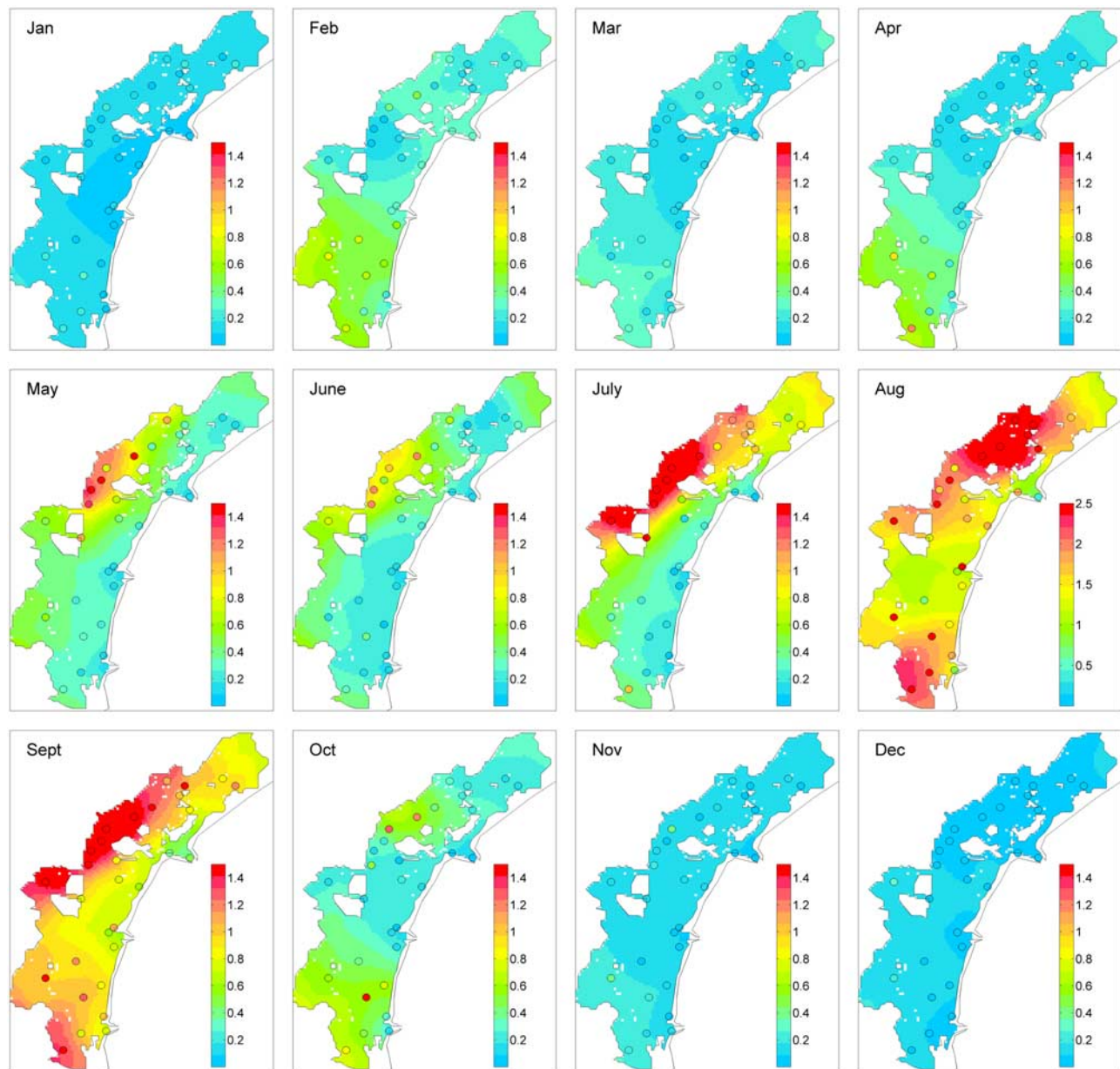
Figure 12. Evolution of the a posteriori fields for phytoplankton (mg/l) (maps) and observation (overlaid colored circles). The color scale is set to 0 to 1.5 mg/l for all months except for August, which has a color scale set to 0 to 2.5 mg/l.

5.2.2. Nutrients: DIN

[48] The results of the twelve monthly a posteriori maps of DIN (Figure 13) show that the spatial patterns are characterized by the presence of two gradients, the northern-center area to center inlets and the southern area to the southern inlet. Specifically, the first gradient is from the rivers located in the northern basin (mainly Dese and Silone) and the area close to P.Marghera toward the inlet of Lido, the central basin and the Malamocco inlet. The second gradient is from the southern area close to the Cuore and Nov.Brenta canals toward the southern Chioggia inlet. Such spatial features are commonly observed in transitional ecosystems where intense gradients are generated between discharge source points and the open ocean [*Cloern*, 2001], but the magnitude and shape of the gradients change from

month to month due to the seasonal evolution of the inputs, in part linked to meteorological forcing. The largest gradients are observed during the winter and fall months when inputs are the highest, biological activity is at the lowest level and internal mixing dynamics drives the spatial distribution of DIN. The highest concentrations, up to 1.3 mg/l are located close to the northern rivers (Dese and Silone) and southern rivers (Cuore and Nov.Brenta) in January, March, April, October, November and December. On the other hand, concentrations lower than 0.4 mg/l are predicted for the same months in the area most influenced by tidal exchanges with the Adriatic Sea.

[49] During the spring and summer, DIN concentrations decrease due to the combined effect of lowering of inputs from rivers and biological uptake. As a consequence the gra-
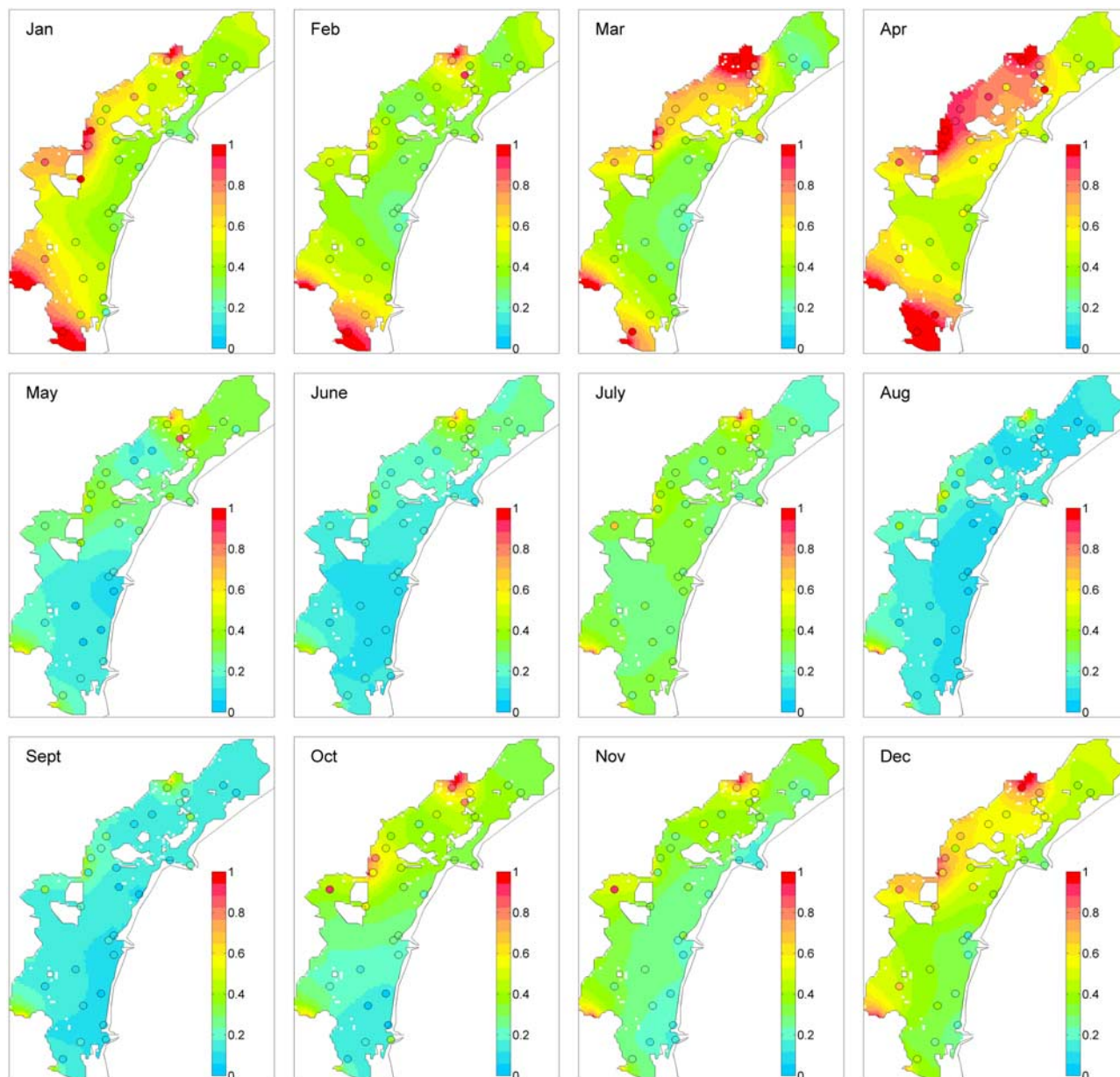
Figure 13. Evolution of the a posteriori fields for DIN (mg/l) (maps) and observation (overlaid colored circles). Color scale is set to 0 to 1 mg/l for all months.

dients are less pronounced, even if some high-concentration spots are still visible near the rivers.

[50] The biggest DA corrections occurred for the area bordered by Venice, Murano and land, where ESSE adequately lowers the higher concentrations simulated by the model during the fall and winter months. A possible underestimation of the diffusivity tensors can be hypothesized for this area that is connected to the Lido inlets by quite narrow but deep and dynamical channels.

5.2.3. Nutrients: DIP

[51] The seasonal evolution of DIP (Figure 14) portrays the same general features observed for the DIN fields. In fact, the sequence of maps of DIP shows the presence of gradients from the input sources (mainly Dese and Silone rivers and industrial area of P.Marghera) toward the Lagoon inlets. However, a significant difference of this general

spatial feature is observed in April, and to a lesser extent in August and May, when a counter gradient, i.e., from the sea to the interior of the Lagoon, is predicted in the central and southern subbasins. This pattern highlights that the Adriatic Sea can be a source of nutrient for some area of the Lagoon and for short periods of time. This finding is in agreement with results other studies: *Sfriso et al.* [1994] adopted an empirical 1 box model even if their estimations were referred to different period of time; *Bianchi et al.* [2004] used observations of nutrient concentration and flux values during a restricted number of tidal events.

[52] With respect to time evolutions, no significant difference of phase between DIP and DIN is found, showing that both nutrients are mainly driven by the same meteorological and ocean boundary forcing. For example, for both nutrients, the highest concentrations are observed during the
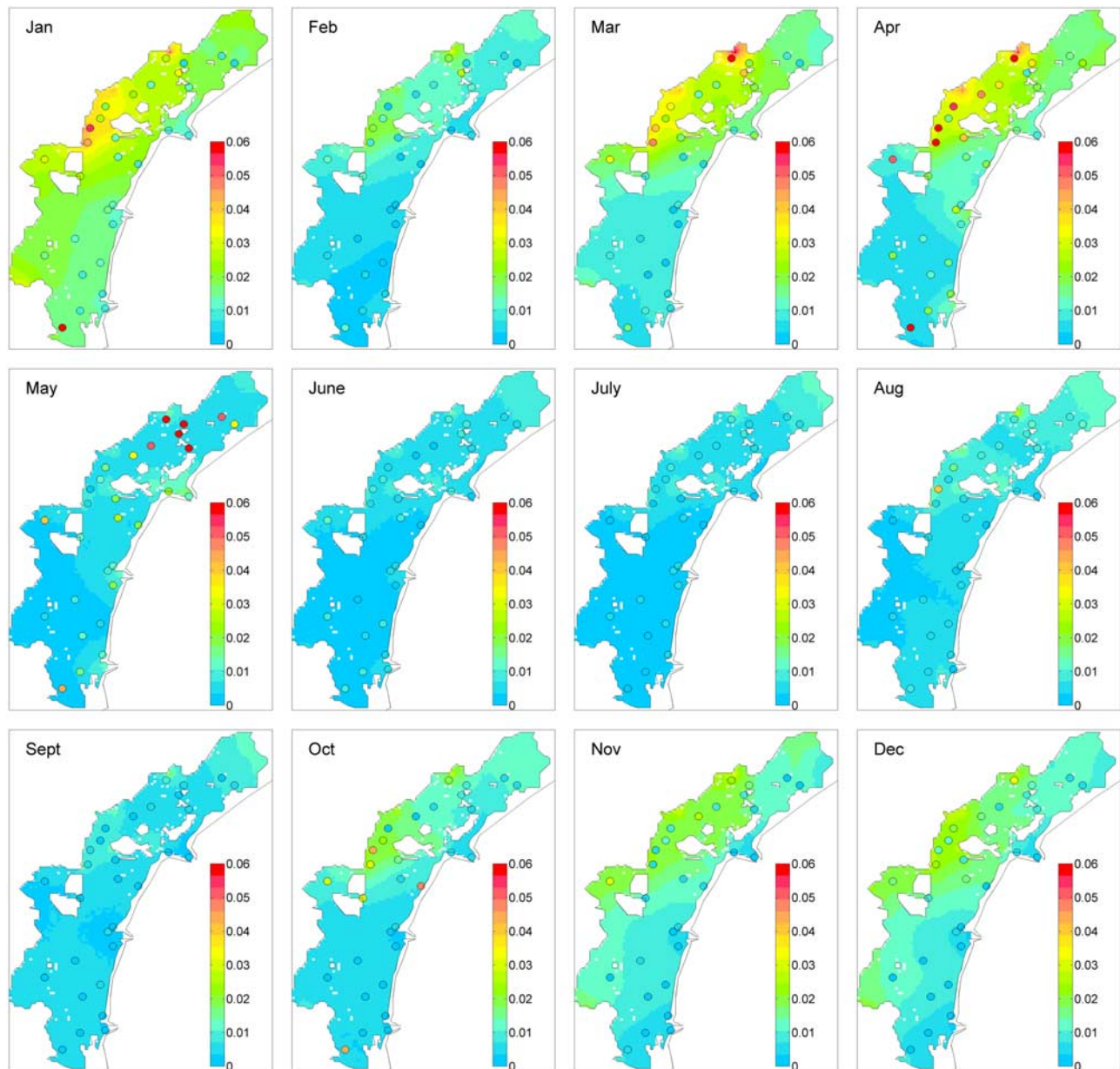
Figure 14. Evolution of the a posteriori fields for DIP (mg/l) (maps) and observation (overlaid colored circles). Color scale is set to 0 to 0.06 mg/l for all months.

spring and fall months while the lowest ones are found during summer months. However, a significant difference between the two nutrients is related to the summer situation. At this time, while the DIN maps still show significant inputs from drainage basin (as in July), the DIP maps report very low concentrations over the whole lagoon. This suggests a possible phytoplankton growth limitation exerted by DIP, and a very fast recycling process for DIP from detritus or sediments, capable of sustaining the intense bloom of July and August. During the last three decades, the concentration of DIP has been showing a negative trend while DIN has not [*Pastres et al.*, 2004], supporting the hypothesis that P has become the limiting nutrient in the Lagoon.

[53] In May, while the observation of DIP in the region of Dese and Silone are up to 0.07 mg/l, the model predictions

(whose a priori values are low) is not corrected by the assimilation. The model-predicted error covariance for this month is low as a consequence of low values and low variability of the discharge evolutions. Consequently the updating has been less effective to what one would have expected. This fact underlines a possible underestimation of the nutrient discharges and of their variability for this month.

5.3. Ecosystem Field Uncertainties and Their Reduction by Data Assimilation

[54] The ESSE error variance forecast, the diagonal of the a priori covariance matrix, complements the eigendecomposition results (section 5.1). For example, the maps of Figure 15 (DIN forecast uncertainties from February to April) show that the larger uncertainties are near the land inflow boundaries. The northernmost region and area
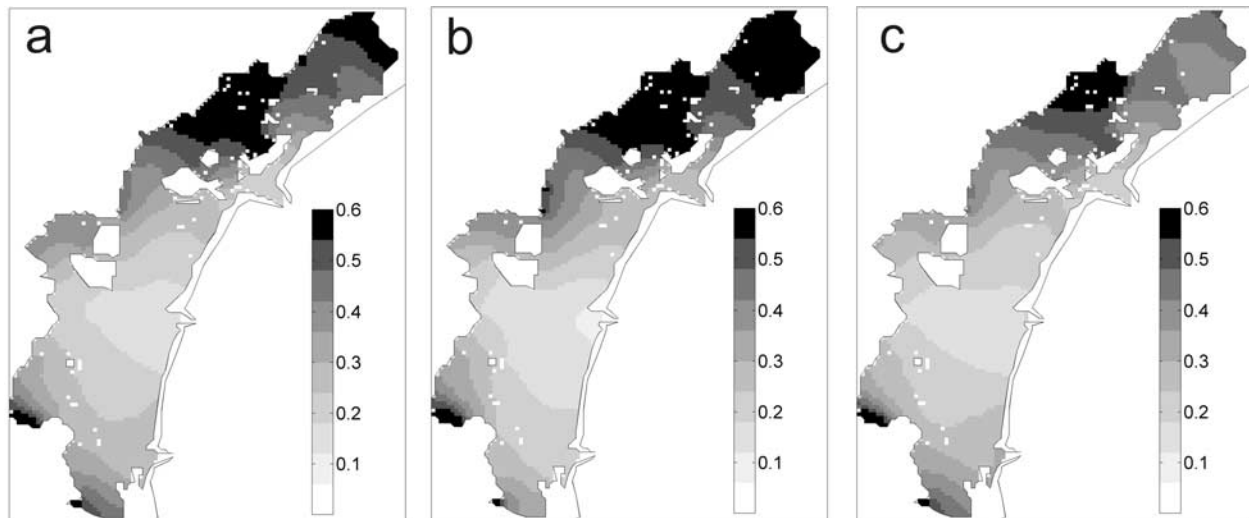
Figure 15. Forecast uncertainties, i.e., the a priori (forecast) error standard deviation (mgN/l) of the forecasted DIN fields of (a) February, (b) March, and (c) April.

north to Venice also show a higher level of uncertainty. This uncertainty mostly results from a combination of the non linear dynamics of the biological model and of the low intensity of the transport-dispersion processes in these regions.

[55] The assimilation significantly reduces these a priori uncertainties. The a posteriori error maps (Figure 16) show a reduction of more than 50% over the whole Lagoon, with decreases up to 80% in the areas close the major sources of uncertainty, e.g., Dese and Silone rivers and P.Marghera industrial area.

[56] The number of sampling points and their spatial spread enables a significant reduction of the model forecast uncertainty for most of the Lagoon. However, there are some differences among the three variables (Figure 17). The highest and most uniform reduction is obtained for DIN. On the other hand, DIP shows an effective reduction only in the northern basin with very small reduction in the southern

basin, in part due to very low DIP concentrations there. The error reduction for phytoplankton is quite similar to that of DIN: both show that only some marginal parts of the Lagoon are less influenced by the assimilation. One is the northernmost part of the lagoon, where the distance from sampling points and the low-intensity hydrodynamics reduce the effectiveness of MELa1 data corrections. Another is the central west Lagoon, because of its small number of data points and their broad scattering. A final one is at the inlets proper, for which the forecasts were already relatively accurate.

6. Assessment of the Water Quality in Relation to the Environmental Legislation: Comparison Between Standard OA Fields and ESSE Fields

[57] Since 1999, to implement the European Union (EU) Directive 96/61 [*EU*, 1996], the Italian Ministries of the
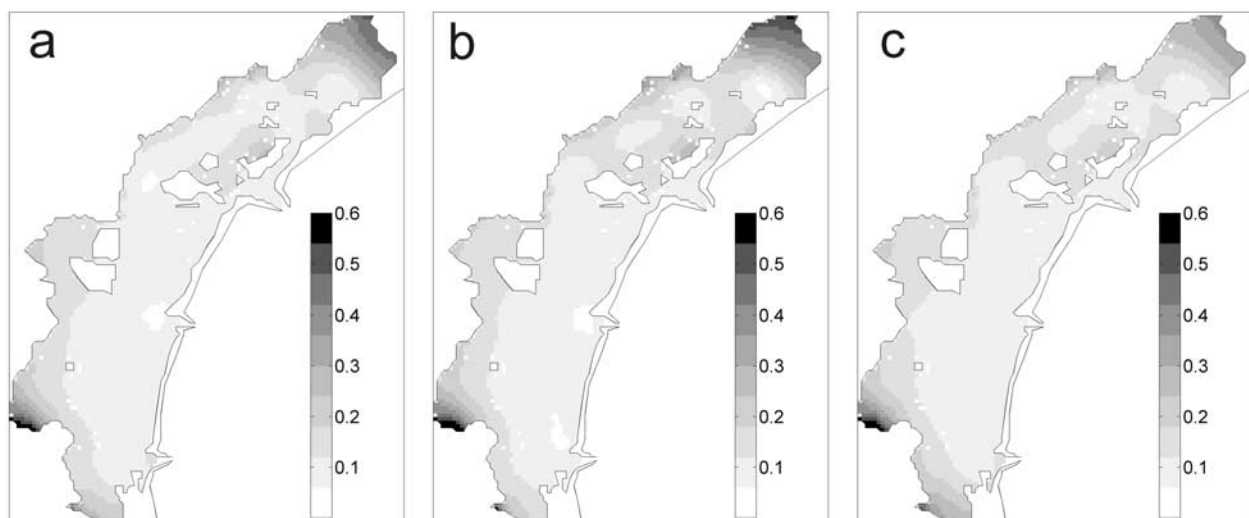

Figure 16. Analyses uncertainties, i.e., the a posteriori (analyzed) error standard deviation (mgN/l) of the updated DIN fields of (a) February, (b) March, and (c) April.
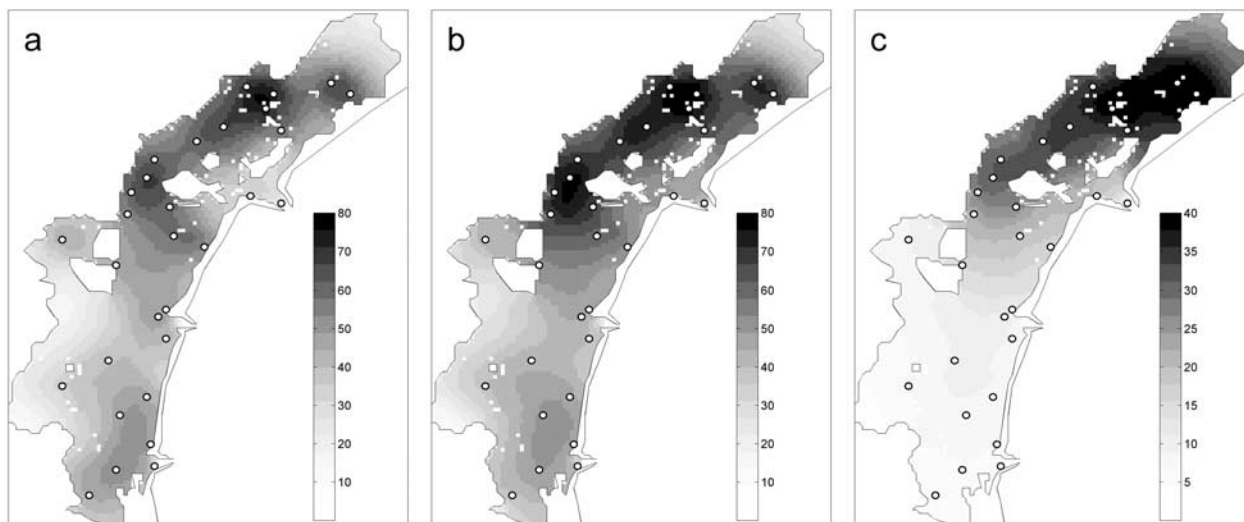
Figure 17. Map of the percentage reduction of the forecast uncertainties for (a) phytoplankton, (b) DIN, and (c) DIP. The map is computed as the mean reduction of the 12 monthly experiments. The location of the sampling station is reported by the white circles.

Environment and Public Works issued a new legislation aimed at the safeguard of the Lagoon of Venice, which established concentration limits of nutrients, N and P, for the Lagoon water, water quality target, and relative maximum permissible loads [*Collavini et al.*, 2005]. The implementation of this policy is challenging due to the high spatial and temporal variability of nutrient patterns [*Solidoro et al.*, 2004] and the difficulty of setting a quantitative relationship among loads and water concentrations [*Pastres et al.*, 2003]. A detailed study of the sources and characteristics of discharged pollutants was recommended [*Collavini et al.*, 2005]. Investigations were carried out to assess the contaminant loads delivered to the Lagoon by different sources, respectively: the industrial area of Porto Marghera [*Magistrato alle Acque di Venezia* (*MAV*), 2000, 2002], the atmospheric deposition [*Guerzoni et al.*, 2005a, 2005b] and the drainage basin [*Zonta et al.*, 2005; *ARPAV*, 2002]. Other efforts also investigated the spatial and temporal variability of the Lagoon's responses to contaminants by means of statistical analysis of the MELa1 data set [*Solidoro et al.*, 2004; *Pastres et al.*, 2004].

[58] The present field reconstruction via ESSE generates a quantitative estimate of the relations between the load levels and the nutrient concentrations in the Lagoon. This estimate is optimal since DA fields integrate the data collected in the Lagoon with the prior knowledge of the ecosystem dynamics and its boundary interactions. For an efficient management of the Lagoon, such estimates of environmental responses to external forcing, as requested by the legislation, are more and more urgent, especially considering anthropogenic activities and climate change [*Scavia et al.*, 2003]. Importantly, ESSE improves standard spatial interpolation methods which do not account for full dynamics [e.g., *Lermusiaux*, 1999a, 1999b, 2001; *Lermusiaux et al.*, 2000]. To illustrate the effects of these improvements, the monthly maps of ESSE and of a standard Objective Analysis (OA) scheme (see Appendix C) were compared and used to evaluate the extent in time and space for which the concentrations of DIN and DIP were above the water quality targets set by the legislation, respectively 0.35 mg/l for DIN and 0.025 mg/l for DIP [*Ministero dell'Ambiente*, 1999].
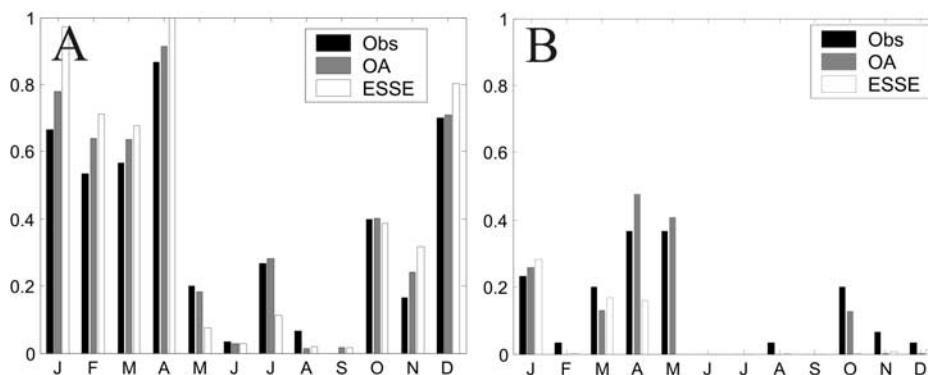
Figure 18. Monthly evolution of the fraction (normalized to 0–1) of the Lagoon that has concentration values above the limit of the water quality standard for (a) DIN and (b) DIP.
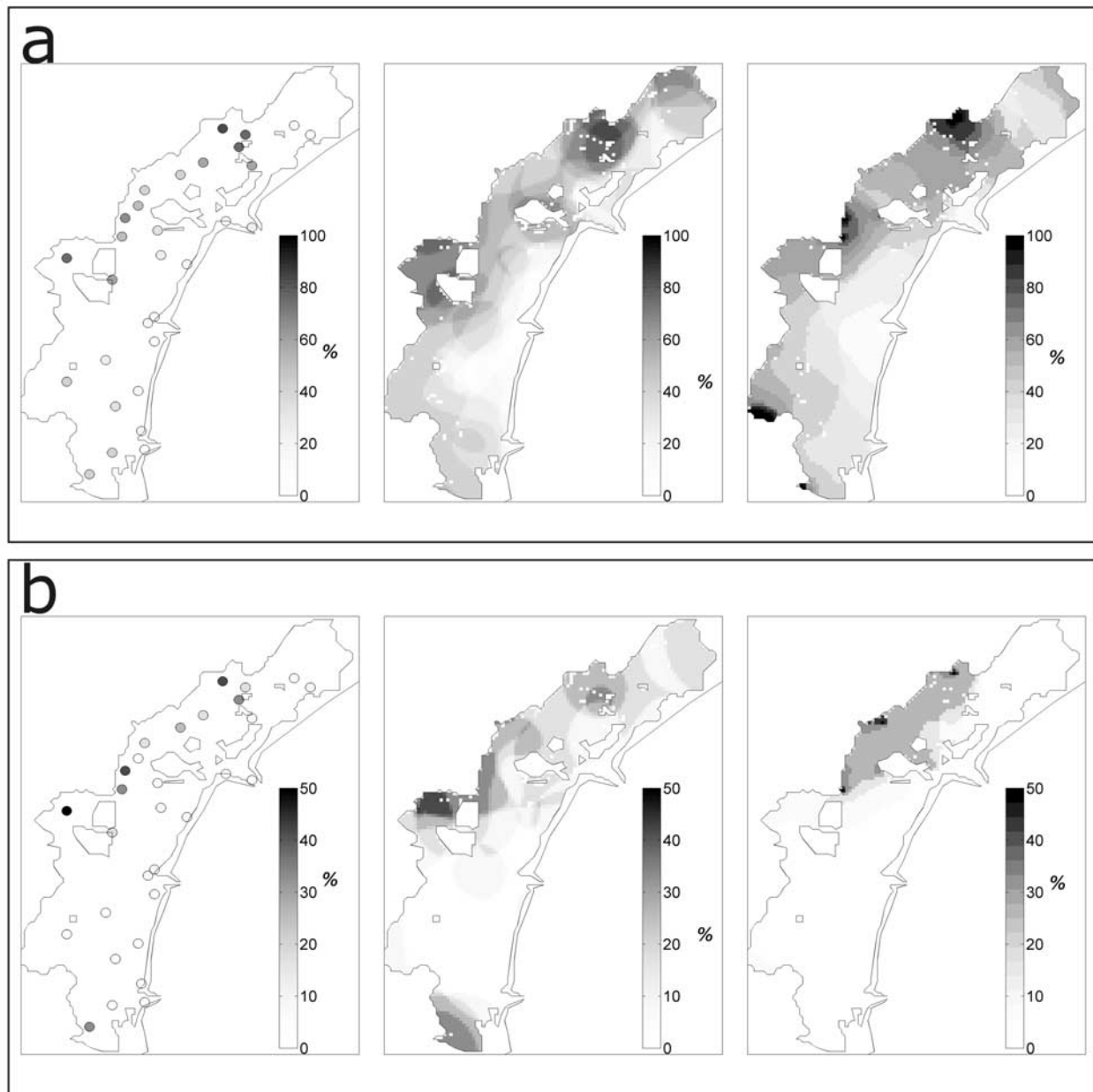
Figure 19. Percentage of time of the year during which the Lagoon is above the limit of the water quality target for (a) DIN and (b) DIP. (left) Data, (middle) OA method, (right) and ESSE method.

[59] The bar plots of Figures 18a and 18b show the fraction of the surface of the Lagoon for which the DIN and DIP concentrations are above the targets, for each of the 12 monthly surveys in 2001. Specifically, shown are the normalized number of times that the 30 observed values (OBS only, black bars) are above the targets and the normalized number of grid points in the OA (gray bars) and ESSE fields (white bars) that have values above the targets. For DIN, the winter, early spring and autumn months exceed the target in more than 50% of the Lagoon surface, with a maximum of 90% during April. The ESSE bars for DIN are often higher than the OBS only and OA ones. This is because ESSE extends the conditions close to the discharge points based on the model dynamics and its uncertainties.

During the summer, most of the Lagoon is under the requested target, and no significant differences are visible among the three estimations.

[60] For DIP, concentrations are low. Never more than 50% of the Lagoon is above the target. Differences between ESSE and the other methods are largest for April, May and October. While in October the difference is due to a few spotty station values, in April and May the difference seems due to an underestimation of simulated discharges of DIP from the northern rivers.

[61] Figures 19a (for DIN) and 19b (for DIP) map the fraction of the year (calculated on the basis of the 12 monthly surveys) during which the water quality target is exceeded. According to the optimal ESSE maps, the areas most subject

to exceed the DIN limits are close to the: discharge points of the rivers Dese and Silone in the northern part of the Lagoon; industrial area of P.Marghera; and, river mouths of Nov.Brenta and Montalbano in the southern basin. Almost all of the northern basin (north of Venice island) and the area in front of P.Marghera exceed the target for more than 50% of the year, while the central part and the area near the channels connecting the inlets are beyond the limit only for a smaller fraction of time. The latter is a result of the dilution by exchanges with the Adriatic Sea. Differences between the ESSE map and the standard OA map are due to strong localized effects that the mosaic of islands, shallow regions and channel areas have on the mixing and dilution dynamics. These dynamics are not included in the simple correlation function used in the standard OA method.

[62] For DIP (Figure 19b), the ESSE map again shows that the areas north of Venice and close to the rivers Dese, Silone and Osellino are the most likely to exceed the water quality target. The spotty gray area in the southern part of OA map is due to the isolated values of a single station (B20) that is located in a very shallow area and close to the discharge point of river Cuori.

7. Summary and Conclusions

[63] An error subspace and ensemble data assimilation scheme (ESSE) was implemented and utilized to study the seasonal ecosystem dynamics of a complex estuary-coastal region, the Lagoon of Venice. The dynamics, given by a physical-biogeochemical model (Trophic Diffusive Model, TDM), was combined with real observations gathered within the framework of a water quality monitoring program (MELa). For the full year 2001, nutrients, plankton and other biogeochemical fields and their prior uncertainties were predicted, and the monthly MELa observations (Chlorophyll-a and dissolved nutrients) assimilated to reduce these uncertainties and estimate forcing parameters. Using the estimated fields and their spatial and temporal variability, the state of the Lagoon was assessed in light of the water quality targets legislations for nutrient concentrations. To our knowledge, this is the first time that both ecosystem fields and their uncertainties were estimated in the Lagoon of Venice using ensemble data assimilation, that ecosystem stochastic models were developed and tuned, that the resulting ecosystem field dynamics were described and studied, and that uncertainties before and after assimilation were computed and analyzed. Key results and findings are summarized next, including opportunities for future research.

7.1. Ecosystem Predictions

[64] Model predictions without assimilation illustrated the main gradients of the ecosystem fields in the Lagoon. Even though the strength of these gradients varied, larger concentrations of nutrients were predicted in the northern part of the Lagoon close to the Dese and Silone rivers, near the Nav.Brenta and Lusore rivers, and in the central part near the industrial area of P.Marghera. The lowest concentrations were near the Lagoon inlets due to the exchanges with the Adriatic Sea. The largest discrepancies with data were often found near the locations of inputs to the ecosystem, e.g., near the industrial areas. These inputs were not well known

a priori. Using Lagoon data and dynamics, a goal of the ESSE assimilation was to correct these external inputs as well as the initial conditions.

7.2. Sensitivity to Input Uncertainties

[65] Before the full assimilation, several sensitivity studies on uncertainty factors and formulations were carried out. First, the sensitivity to the initial uncertainty was quantified. Ensembles of stochastic initial conditions (ICs) were created for each month and a deterministic TDM with fixed a priori forcing was integrated forward to the next month from each of these ICs. Studying the variance fields of these 12 ensembles showed that: (1) the spatially averaged variance decayed with time, often exponentially; and, (2) the temporally averaged variance decayed the fastest near the boundary inputs (inlets and discharges) and the slowest in the marginal or internally active areas (e.g., northern basin and western part). DIN variances were found to decay faster than DIP and phytoplankton variances. On average, about 75% of the initial ecosystem variability was dissipated after one month. To confirm this, fields of half-decay characteristic times were computed. They were found to be around 10 to 20 days in several regions, and only reached more than 20 days in the northernmost region. General results are that boundary conditions (BCs) and internal mixing have a significant control on the solution, limiting the influence of the initial variability, and that the corresponding uncertainties in the BCs and internal model thus need to be simulated.

7.3. Stochastic Ecosystem Models

[66] To represent uncertainties, a novel stochastic formulation of the ecosystem model including stochastic BCs was implemented and utilized with ESSE. The stochastic forcing are additive and multiplicative random fields that are appended to the original model and its BCs. Several stochastic formulations were tested and tuned so as to obtain ESSE uncertainty predictions that are compatible with data-model misfits. For the internal model errors, correlations are needed to model uncertainties in the biogeochemical patchiness at subgrid scales and in the inhomogeneous and anisotropic parameterization of tidal effects. It was found that these internal uncertainties could be modeled by zero-mean normal processes, with a 10% relative amplitude and about 1 km patchy spatial scale. For the boundary uncertainties, zero-mean normal processes were also found acceptable but with a 60% relative amplitude and about 1-month decorrelation time scale. Ensembles of simulations were carried out for each of the 12 monthly assimilation periods, so as to confirm the suitability of these internal and BC error models. With these error models, the highest uncertainties were predicted in the central and northern regions of the Lagoon.

[67] The required size of the ESSE ensemble was then computed based on a convergence criterion. Even though in real-time this size could have been optimized [e.g., *Lermusiaux*, 1999b, 2001, 2002] for each state variable and monthly dynamics, in our hindcast studies, the largest common size needed, 220, was chosen for all variables and all months.

[68] For the measurement model, several additive and multiplicative errors were tested and tuned based on a series

of data assimilation tests. Suitable amplitudes were found to be a 10% relative error for each measured variable combined with an absolute error of standard deviation of 0.025, 0.025 and 0.005 mg/l for phytoplankton, DIN and DIP, respectively.

7.4. Dominant Uncertainty Modes

[69] The singular vectors of the ESSE ensemble identified the patterns where the largest uncertainties occurred in 2001. For DIN, the two major rivers (Dese and Silone in the northern lagoon) were found to be the largest sources of uncertainty. In the maps of the second DIN vector, other sources were identified, corresponding to diverse boundary points from month to month, e.g., the southern rivers or the industrial discharges. These second vectors were either decoupled or in opposition of phase with the first "major rivers" mode. The full field model-point results of the ESSE vectors agreed with data EOFs at data points. For the other variables (DIP and phytoplankton), the ESSE and EOFs results also had dominant modes linked to external boundaries, but their internal dynamics was more significant than for DIN. Prior and posterior ESSE uncertainty estimates agreed with these findings.

7.5. Variability of Ecosystem Fields

[70] The quantitative estimates of the ecosystem fields after ESSE assimilation cover the whole Lagoon and allow novel descriptions of the ecosystem during 2001. The Lagoon is characterized by the presence of nutrient and phytoplankton gradients from its inshore regions toward the areas influenced by exchanges with the Adriatic Sea. The mean concentration level, and the intensity and shape of gradients, varies from month to month according to the evolutions of boundary and surface forcing, and internal dynamics. The largest gradients occur during the winter and fall, when inputs are high, biological dynamics is low and physical mixing is a main internal driver. Concentrations of nutrients (DIN and DIP) are the lowest during the summer due to the combined effects of lower rivers discharges and enhanced biological uptake by primary producers. A late-spring phytoplankton bloom starts in the northern Lagoon in May (where nutrients are supplied) and spreads over the whole Lagoon during the summer, with concentrations up to 2.5 mg/l in August. This August bloom is found to be sustained through rapid regeneration and recycling processes from detritus and sediments, with very low nutrient concentrations, especially for DIP which is limiting in summer. It is also shown that the Adriatic Sea can be a source of nutrient for parts of the Lagoon and for short periods of time, specifically for DIP in April and to a lesser extent in May and August.

7.6. Uncertainty Reductions and Data Impacts

[71] The largest ESSE correction to the a priori state occurred in the phytoplankton mean level in August during the summer bloom and locally in the southern region in February during a late winter bloom. These corrections reflect the capacity of ESSE to correct for boundary river and industrial forcing, but also to remedy for inaccuracies in parameter values (e.g., maximum growth rate of phyto-

plankton) and simplifications in model formulations (e.g., use of a single pool of primary producers instead of several). The largest corrections to nutrients were found in marginal areas, where turbulent diffusivity is not well resolved. Other corrections were estimated in areas close to specific point sources on a few months. Uncertainties are estimated to be reduced by data assimilation by about 50 to 80%. Data impacts show that the density of the MELa1 sampling should be increased in the northernmost and central west portions of the Lagoon.

7.7. Water Quality

[72] Our field estimation merged data and models to quantify relations between load levels and nutrient concentrations in the Lagoon, as recommended by water quality target directives. The extent in time and space for which ESSE fields of DIN and DIP were above these targets was computed. It was also compared to that obtained using data-only values and a standard objective analysis (OA) of these data. Differences are due to the dynamical interpolation of the data using tuned multivariate ESSE covariances and to localized dynamics in the complex Lagoon geometry. On certain months, they are also due to strong data outliers. For DIN, the winter, early spring and autumn months exceed the target in more than 50% of the Lagoon, but in summer, most of the Lagoon is under the target. For the more often limiting DIP, concentrations are lower and never more than 50% of the Lagoon is above the target.

7.8. Future Research

[73] Research opportunities and applications abound over a rich spectrum of needs. Future work includes the application of ESSE to other years and periods in the Lagoon. A sustained adaptive recalibration [*Lermusiaux*, 2007] of the biogeochemical-ecosystem model parameters and parameterizations as well as a study of the corrections to the a priori boundary forcing by ESSE assimilation could also be explored. Detailed investigations of the Lagoon's ecosystem dynamics such as term-by-term balances and computations of fluxes, exchanges and transfer rates, should also be carried out. Other possibilities involve the use of a 4D hydrodynamic model in the Lagoon, with 2-way nesting within a full Adriatic model [*Pinardi et al.*, 2002; *Oddo et al.*, 2006] and barotropic tidal forcing [*Logutov and Lermusiaux*, 2008]. In the ecosystem model, bacteria, benthic microalgae and filter feeders could be included and recycling processes better formulated. Multimodel estimates are also possible [*Logutov*, 2007; *Rixen et al.*, 2008]. Effects of shorter scales and larger scales including climate influences [*Pinardi et al.*, 2005; *Cossarini et al.*, 2008] could also be explored.

[74] Our results suggest that the frequency of monitoring surveys should be increased. It has in fact already doubled in spring and summer. In the future, our novel combination of data and models using ESSE could be used for sustained management and forecasting of the Lagoon, in accord with water quality targets. Such societal applications would be unprecedented and of critical importance to the region and its multiple industries. Related research areas include optimum combinations of fixed and adaptive sampling of the ecosystem [*Lermusiaux et al.*, 2007], possibly using auton-
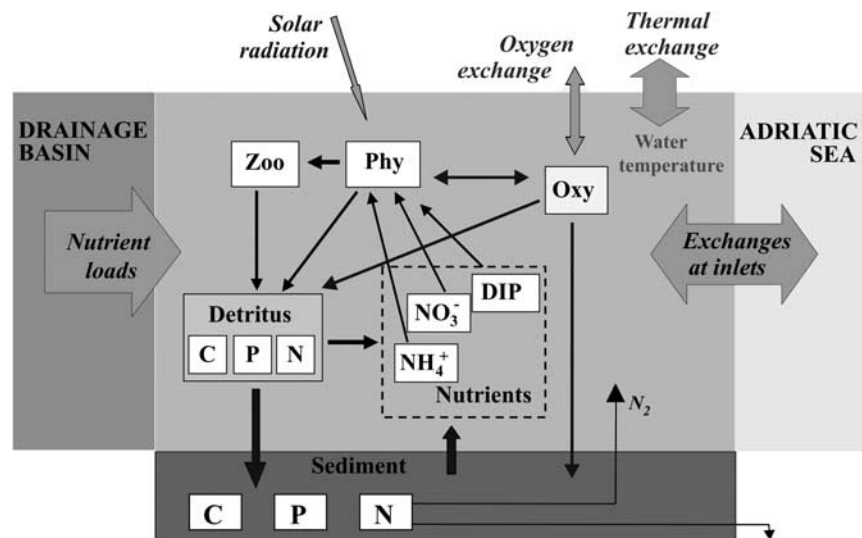
Figure A1. Scheme of the biogeochemical model and interactions used for the Lagoon of Venice. Shown are the compartments of the ecosystem description and the exchanges between the system and the outside environment: sediment, air, drainage basin, and the Adriatic Sea.

omous assets [*Yilmaz et al.*, 2008; *Wang et al.*, 2009] and real-time observation systems [*Ciavatta et al.*, 2004].

Appendix A: Model Formulation

A1. Biological Model

[75] The Trophic Diffusive Model (TDM) describes the evolution of 13 state variables in space and time in the 3 dimensional domain of the Lagoon of Venice according to the equation

$$\frac{\partial C_i}{\partial t} = w_{si} \frac{\partial C_i}{\partial z} + \nabla_H K_h \nabla_H C_i + \frac{\partial}{\partial z}\left[K_v \frac{\partial C_i}{\partial z}\right] + R_i(C, T, I, ..)$$

(A1)

where C_i is the concentration or density of a given state variable in the water column, w_{si} its sinking velocity, K_h and K_v the horizontal and vertical eddy diffusion coefficient, R_i the reaction term and T and I indicate, respectively, water temperature and Irradiance. The numerical solution of the governing equation (A1) is computed using a finite difference approach. The Lagoon spatial domain is subdivided in a regular grid (horizontal resolution of 300 m × 300 m, and vertical resolution of 1 m). This leads to a number of $103 \times 140 \times 5$ discrete model points. Because of the shallow Lagoon, only 7825 of these discrete points correspond to active cells, 4369 of which correspond to the first meter. The integration time step is 1 hour, resolving diel processes.

[76] The set of state variables includes phytoplankton, zooplankton, nutrients (dissolved inorganic phosphorus, ammonium and nitrate), nutrient content in detritus (DetC, DetN, DetP), sediments (SedC, SedN, SedP), dissolved oxygen and Temperature (Table A1 and Figure A1). The R_i term in equation (A1) describes the growth and loss terms of each variable and the main interactions among the variables. The growth of phytoplankton, that is thought to have a C:N:P Redfield fixed ratio, is described using a

multiplicative model including a Michaelis-Menten formulation [*Michaelis and Menten*, 1913] for nutrients, a Steele formulation [*Steele*, 1962] for light limitation and a Lassiter and Kearns formulation [*Lassiter and Kearns*, 1974] for temperature limitation. Loss terms of phytoplankton include extracellular exudation, grazing and mortality. Zooplankton feeds on phytoplankton, using a Holling III type formulation [*Holling*, 1965], and channels carbon and nutrients mainly toward the detritus compartment, through excretion, mortality and sloppy feeding processes. Detritus and phytoplankton sink and eventually enter the surface sediment state variable. The remineralization rate of the organic matter, which takes place both in the water column and in the surface sediments, depends on temperature and dissolved oxygen availability. This process involves the consumption of dissolved oxygen and leads to the release of inorganic nutrients back to the water column. Phytoplankton and zooplankton respirations, photosynthesis and air-sea exchanges are the other processes involved in the dissolved oxygen budget. Denitrification and sediment burial are also taken into account. All details on the model formulations are provided by *Solidoro et al.* [2005a].

Table A1. List of the State Variables

	State Variables	Unit
Phy	Phytoplankton	mgC/l
Zoo	Zooplankton	mgC/l
NH_4^+	Ammonia	mg/l
NO_3^-	Nitrate	mg/l
DIP	Dissolved inorganic phosphorus	mg/l
Oxy	Dissolved oxygen	mg/l
T	Temperature	°C
DetC	C in detritus	mg/l
DetN	N in detritus	mg/l
DetP	P in detritus	mg/l
SedC	C in sediment	mg/m^2
SedN	N in sediment	mg/m^2
SedP	P in sediment	mg/m^2

Table A2. Nutrient N and P loads and Indication of the Typology of Discharge Sources and Frequency of the Data or Estimations

	DIN (tN/a)	DIP (tP/a)	Typology	Frequency of the Data or Estimation
Silone	743	19	River	Monthly
Dese	636.5	17.4	River	Monthly
Osellino	123.4	3.9	River	Monthly
Campalto	86.7	15	Sewage treatment plant	Yearly
Venezia	405.5	47.4	Urban sewage systems	Yearly
Murano	45.9	5.4	Urban sewage systems	Yearly
Cavallino	9	1	Urban sewage systems	Yearly
Lusore	364.7	7.3	River	Monthly
Nav.Brenta	542.8	8.1	River	Monthly
P.Marghera	450.7	15	Industrial Area and sewage treatment plant	Yearly
Lova	94.2	1.7	River	Monthly
Nov.Brenta	378	4.5	River	Monthly
Montalbano	36.2	0.9	River	Monthly
Cuori	184.9	1.1	River	Monthly
Chioggia	55.8	11	Urban sewage systems	Yearly
Air deposition	556	48	Diffuse	Yearly

A2. Transport Model

[77] The transport model describes processes which are characterized by time scales larger than the tidal period; averaging over a tidal cycle, the residual currents can then be considered instead of the actual currents [*Sin and Wetzel*, 2002]. Since the residual currents are here almost everywhere very small [*Dejak et al.*, 1998], most of their effects can be neglected. Transport processes are thus described by means of a turbulent diffusion module and residual advection is not explicitly taken into account. However, diffusion processes are no longer isotropic and homogeneous. They are parameterized at each grid points [*Dejak et al.*, 1998; *Pastres et al.*, 2001]. The turbulent diffusivity coefficients K_h in equation (A1) are replaced by a diagonal tensor, which relates the fluxes of matter Φ to the gradients of the concentration along the main direction of dispersion (x′) and its orthogonal one (y′), as written next in equation (A2a)

$$\begin{vmatrix} \Phi_{x'} \\ \Phi_{y'} \\ \Phi_z \end{vmatrix} = \begin{vmatrix} K_{x'x'} & 0 & 0 \\ 0 & K_{y'y'} & 0 \\ 0 & 0 & K_{zz} \end{vmatrix} \begin{vmatrix} \partial C/\partial x' \\ \partial C/\partial y' \\ \partial C/\partial z \end{vmatrix} \quad (A2a)$$

[78] The tensor coefficients in (A2a) are estimated once for all, and for each grid point one at a time, by using a precomputed total velocity field obtained under nominal conditions of tidal forcing and wind forcing (cyclic tides, no winds). Then, since equation (A2a) describes appropriately the transport processes in the local reference systems x′, y′ relative to each grid point, a proper rotation is applied to each tensor, in order to describe diffusion from all points in a common reference system x − y [*Dejak et al.*, 1998; *Pastres et al.*, 2001]. The horizontal and vertical diffusion have different time and spatial scales and are therefore treated separately.

$$\begin{vmatrix} \Phi_x \\ \Phi_y \\ \Phi_z \end{vmatrix} = \begin{vmatrix} K_{xx} & K_{xy} & 0 \\ K_{yx} & K_{yy} & 0 \\ 0 & 0 & K_{zz} \end{vmatrix} \begin{vmatrix} \partial C/\partial x \\ \partial C/\partial y \\ \partial C/\partial z \end{vmatrix} \quad (A2b)$$

A3. Energetic Model

[79] The spatial and temporal evolution of the water temperature is computed by means of an energetic submodel [*Dejak et al.*, 1992], while that of light intensity is computed within the biological module, since light attenuation along the water column is a function of water quality properties. Data of air temperature, short-wave radiation, cloud cover, air pressure and air humidity, used in the energetic submodel were collected by the Marine science institute ISMAR-CNR (National Research Council) of Venice, see http://www.istitutoveneto.it/.

A4. Boundary Conditions

[80] Heat discharges from the power plant of P.Marghera are computed on the basis of the data reported the study of *Socal et al.* [1999]. Other inputs of energy or mass, as well as exchanges through open boundaries are taken into account by specifying appropriate boundary conditions. The model uses two types of boundary conditions: Dirichlet at the three inlets and Neumann at the rivers and discharge points boundaries.

[81] For the three inlets (Figure A1), a data-based, daily reference evolution is assigned for the horizontal fluxes of the state variables. This is done at the grid cells that define each of the three boundaries between the lagoon and the Adriatic Sea. Then the exchange fluxes are computed as

$$\Phi_{inlet} = K_h \cdot \frac{(C - C(t)|_{x=inlet})}{\Delta x} \quad (A3)$$

where $C(t)|_{x=inlet}$ is a measured reference daily evolution of the state variable at the boundary, C the concentration of the state variable in the inner adjacent grid point, and K_h the horizontal eddy diffusion coefficient at the boundary. The three different reference evolutions (one for each of the three inlets) are obtained for phytoplankton, nutrients and temperature by spline interpolation of the monthly MELa1 observations at six neighboring stations. These stations, located near the three inlets, have been showed to be the most representative of the quality of the marine water [*Solidoro et al.*, 2004]. The inlet BCs for zooplankton are

assumed to be equal to 0.1 of the inlet BCs of phyto-plankton. Dissolved oxygen at the inlet is set to its saturation level [*Melaku Canu et al.*, 2001] and N and P contents of detritus are assumed constant [*Bergamasco and Zago*, 1999].

[82] The rivers and discharges are mainly in the northern and western side of the lagoon. There are nine rivers, two sewage treatment plants and four urban areas and an indus-trial area (Figure 1) that discharge a considerable amount of nutrients in the lagoon, respectively 4.7×10^6 Kg/y of nitrogen and 0.2×10^6 Kg/y of phosphorus. For 2001, monthly estimations are available for the nine rivers [*ARPAV*, 2002] and annual mean values are used for the sewage systems and urban areas [*MAV*, 2002; *Melaku Canu et al.*, 2001; *Sezione Antinquinamento del Magistrato alle Acque (SAMA)*, 2003]. Table A2 reports the annual mean load of nitrogen and phosphorous of the 15 discharge sources among which the rivers Dese, Nav Brenta and Lusore, and the direct discharges from Venice's historical center and industrial area are the most important. Atmo-spheric deposition is significant too, but it does not play any important role at local level.

[83] It is necessary to represent the variability with respect to these mean values (Table A2). This is because it has been observed that intense rainfall events (that can exceed 100 mm/d [*Zuliani et al.*, 2005]) are associated with very large amounts of nutrient transported by the river discharges into the lagoon [*Rinaldo et al.*, 2006; *Botter et al.*, 2006]. Further, a significant fraction of the total annual load can be due to these few flood days [*Collavini et al.*, 2005]. Therefore we developed a new empirical boundary formulation that links the k river discharges $\Phi_C(k)$ to the evolution of the daily precipitation

$$\Phi_C(k) = \overline{\Phi_C} \cdot f_R(k) \tag{A4}$$

where $\overline{\Phi_C}$ is the value of the monthly (or annual) data. The function f_R, whose monthly integral is equal to 1, accounts for the fact that when it rains there is a significant increase of the load, while when it does not rain, the discharge is below the monthly mean. It is defined by

$$f_R(k) = 1 + \frac{r_{k-1} - \langle r_k \rangle_{month}}{\max(\{r_k\}_{month}) - \langle r_k \rangle_{month}} \cdot \beta_{source} \tag{A5}$$

where $\langle r_k \rangle_{month}$ is the mean monthly precipitation and $\max(\{r_k\}_{month})$ is the maximum precipitation during the month. A lag time of one day between rain and discharge is used because of the drainage basins are not wide and runoff of rivers follows quickly the rainfall events [*Zuliani et al.*, 2005]. The denominator is a normalization factor. The parameter β_{source} is equal to 1 for rivers and atmospheric deposition, and 0.50 for sewage systems and urban areas, and it accounts for the different response of the given typology of discharge sources to the rainfall. Finally a random noise is added to this parameter in order to take into consideration its uncertainty. These stochastic components of the boundary conditions are discussed in the text.

A5. Model Evaluation

[84] In the work of *Solidoro et al.* [2005a], the TDM model results were compared to three different data sets for year 1998, and to information concerning flow rates obtained from the literature. The comparisons showed that the model reproduced the spatial gradients of nutrients concentration well and also mimicked reasonably the principal features of the timing and magnitude of phytoplankton blooms. Overall, the model results were in general agreement with the exper-imental findings on nitrogen fluxes collected in the Lagoon of Venice during the 1990s.

Appendix B: Error Subspace Statistical Estimation: Ensemble Prediction and Melding Steps

[85] The main ESSE components are: (1) uncertainty initialization; (2) deterministic-stochastic ensemble and error subspace forecasts; (3) adaptive sampling; (4) data processing and measurement model; (5) data assimilation; (6) adaptive error learning; and, (7) smoothing. Here, we summarize the prediction (1, 2) and assimilation (5) steps which are the main ESSE schemes used in our study. We refer to the work of *Lermusiaux et al.* [2002] and *Lermusiaux* [1999a, 1999b, 2002, 2006, 2007] for more detailed descriptions of all ESSE components.

B1. Ensemble and Error Subspace Prediction

[86] Presently, an ensemble of stochastic model simula-tions, initialized based on an estimate of the dominant initial uncertainties, is used to predict the error subspace of the model fields. For minimum error variance estimation, the error subspace is defined by a truncation of the ordered eigendecomposition of the nondimensionalized multivariate error covariance matrix. At time t_k, the model state analysis $\hat{\mathbf{x}}_k(+)$ (the posterior state) is perturbed (B1a) using the dominant eigenvectors $\mathbf{E}_k(+)$ of the posterior error covari-ance matrix. To do so, random coefficients $\pi_k^j(+)$ function of the dominant eigenvalues $\mathbf{\Pi}_k(+)$ and constrained by dynam-ics are utilized. Random white noise $\mathbf{n}_k^j$ is also added to model the tail of the error spectrum which is truncated by ESSE. To evolve fields and uncertainties up to t_{k+1}, an ensemble of $j = 1, \ldots, q$ stochastic ocean model integrations is carried out, see (B1b) where M represents the dynamical model. This ensemble is started from the q perturbed states $\hat{\mathbf{x}}_k^j(+)$. The new stochastic forcing $d\boldsymbol{\eta}$ that we developed for the Lagoon's ecosystem are defined in section 4 of the main text

$$\hat{\mathbf{x}}_k^j(+) = \hat{\mathbf{x}}_k(+) + \mathbf{E}_k(+)\pi_k^j(+) + \mathbf{n}_k^j \quad j = 1, \ldots, q \tag{B1a}$$

$$\hat{\mathbf{x}}_{k+1}^j(-)|d\hat{\mathbf{x}}^j = \mathcal{M}(\hat{\mathbf{x}}^j, t)dt + d\boldsymbol{\eta} \quad \text{with} \quad \text{IC}: \ \hat{\mathbf{x}}_k^j = \hat{\mathbf{x}}_k^j(+) \tag{B1b}$$

$$\mathbf{M}_{k+1}(-) = \left[\hat{\mathbf{x}}_{k+1}^j(-) - \hat{\mathbf{x}}_{k+1}^{em}(-) \right] \tag{B1c}$$

Table C1. Set of Correlation Parameters (Length Scales) Estimated for the Objective Analysis

Variable	a (km)	b (km)
DIN	3	12.5
DIP	4	10.0
Phytoplankton	2	12.5

$$\left\{\sum\nolimits_{k+1}(-), \mathbf{E}_{k+1}(-)\right\} \mid \mathrm{SVD}_p(\mathbf{M}_{k+1}(-))$$
$$= \mathbf{E}_{k+1}(-)\sum\nolimits_{k+1}(-)\mathbf{V}_{k+1}^T(-) \quad (\text{B1d})$$

$$\rho = \frac{\sum_{i=1}^{\min(\tilde{p},p)}\sigma_i\left(\mathbf{\Pi}^{1/2}\mathbf{E}^T\tilde{\mathbf{E}}\tilde{\mathbf{\Pi}}^{1/2}\right)}{\sum_{i=1}^{\min(\tilde{p})}\sigma_i(\tilde{\mathbf{\Pi}})} \leq \alpha \quad (\text{B1e})$$

[87] The error subspace forecast (B1c)−(B1e) is obtained from this ensemble. First, a matrix $\mathbf{M}_{k+1}(-)$ which contains the difference between the available q model state realizations at t_{k+1} and the corresponding estimate of the conditional mean, $\hat{\mathbf{x}}_{k+1}^{em}(-) = E^q\{\hat{\mathbf{x}}_{k+1}^j(-)\}$, is computed (B1c): $\mathbf{M}_{k+1}(-) = [\hat{\mathbf{x}}_{k+1}^j(-) - \hat{\mathbf{x}}_{k+1}^{em}(-)]$. It is subsequently normalized and decomposed by singular value decomposition (B1d) into $\mathbf{\Pi}_{k+1}(-) = \frac{1}{q}\mathbf{\Sigma}_{k+1}^2(-)$ and $\mathbf{E}_{k+1}(-)$ of rank $p \leq q$. In (B1d), the operator SVD_p (.) selects the rank p SVD. The ensemble size is subsequently increased and ultimately controlled by a convergence criterion (B1e) which measures the similarity between two subspaces of different sizes [*Lermusiaux*, 2007]. A "previous" estimate $(\mathbf{E}, \mathbf{\Pi})$ of rank p and "new" estimate $(\tilde{\mathbf{E}}, \tilde{\mathbf{\Pi}})$ of rank $\tilde{p} \geq p$ are compared, using singular values to weight singular vectors. In (B1e), α is a scalar close to one that is chosen by the user and $\sigma_i(\cdot)$ selects the singular value number i. When the scalar ρ is close enough to one, the two subspaces are similar in the variance explained sense. The resulting $\tilde{\mathbf{\Pi}}$, $\tilde{\mathbf{E}}$ is then chosen as the error subspace forecast for t_{k+1}: $\mathbf{\Pi}_{k+1}(-)$, $\mathbf{E}_{k+1}(-)$. The dimensions of the ensemble q and subspace p vary with time, in accord with data and dynamics.

B2. Data Assimilation (Melding)

[88] Once the error subspace forecast (B1e) is available, the data $\mathbf{y}°$ and model estimates $\hat{\mathbf{x}}(-)$ can be combined by minimum error variance estimation. This data assimilation step (2a−d) is similar to the classic Kalman update, excepted that the error covariance is replaced by an estimate of its dominant eigendecomposition.

$$\hat{\mathbf{x}}(+) = \hat{\mathbf{x}}(-) + \mathbf{K}^p(\mathbf{y}° - \mathcal{H}(\hat{\mathbf{x}}(-))) \quad (\text{B2a})$$

$$\mathbf{K}^p = \mathbf{E}_-\mathbf{\Pi}(-)\mathbf{E}_-^T\mathbf{H}^T\left(\mathbf{H}\,\mathbf{E}\,\mathbf{\Pi}(-)\mathbf{E}_-^T\mathbf{H}^T + \mathbf{R}\right)^{-1} \quad (\text{B2b})$$

$$\mathbf{L}\,\mathbf{\Pi}(+)\mathbf{L}^T = \mathbf{\Pi}(-) - \mathbf{\Pi}(-)\mathbf{E}_-^T\mathbf{H}^T$$
$$\times \left(\mathbf{H}\,\mathbf{E}\,\mathbf{\Pi}(-)\mathbf{E}_-^T\mathbf{H}^T + \mathbf{R}\right)^{-1}\mathbf{H}\,\mathbf{E}\,\mathbf{\Pi}(-) \quad (\text{B2c})$$

$$\mathbf{E}_+ = \mathbf{E}_-\mathbf{L} \quad (\text{B2d})$$

In (B2a)−(B2d), the subscript $k+1$ has been omitted, $\mathbf{E}_\pm = \mathbf{E}_{k+1}(\pm)$ and $\mathbf{\Pi}_\pm = \mathbf{\Pi}_{k+1}(\pm)$. The outputs of (B2a)−(B2d) are the posterior (filtering) estimates: the fields $\hat{\mathbf{x}}_{k+1}(+) = \hat{\mathbf{x}}(+)$ and error subspace covariance $\mathbf{\Pi}_{k+1}(+)$, $\mathbf{E}_{k+1}(+)$. These estimates can also be obtained from a direct update of the SVD of the ensemble spread, e.g., *Lermusiaux and Robinson* [1999].

Appendix C: Objective Analysis Scheme

[89] DIN, DIP and chlorophyll data of MELa1 data set are spatially interpolated to the model grid using a classic mapping scheme [*Bretherton et al.*, 1976], so as to allow comparisons with the data-dynamics melded estimates of ESSE (a time-space dynamic extension of the diffusion scheme of *Lynch and McGilicuddy* [2001]). Chlorophyll-a measurements are first converted to phytoplankton biomass using the formulation proposed by *Cloern et al.* [1995]. The spatial interpolation of the measurements is produced by objective analysis, in accord with the optimal linear Gauss-Markov theorem. The result is the OA field.

$$\Psi_{OA,x} = \sum_{q=1}^{N} C_{x,q} \cdot \left(\sum_{s=1}^{N} CC_{q,s}^{-1} \cdot y_s\right) \quad (\text{C1})$$

where $C_{x,q}$ is the spatial correlation function between grid point x and measurement location q, $CC_{q,s}$ is the covariance matrix between measurement locations, and y_s is the anomaly of the observations from a background (monthly mean of observations). The background is ultimately added after OA. The correlation function [*Lermusiaux*, 1999a] adopted is isotropic and homogeneous over the domain

$$C_r = \left(1 - r^2/a^2\right) \cdot e^{-\frac{r^2}{2b^2}} \quad (\text{C2})$$

where a is the zero-crossing distance and b the spatial decay scale and r is the Euclidian distance between two point. The two parameters a and b in (C2) are estimated using the MELa1 data set; for each of the 3 variables considered, the correlations between the detrended time series of all the possible couples of sampling locations are plotted versus their Euclidean distances, then the two parameter are computationally estimated in a minimum least square root sense. The values of the parameters are reported in Table C1 below:

[90] These values meet the condition $a > 2^{1/2}b$ to generate a positive-definite correlation matrix [*Artegiani et al.*, 1997]. The analysis of Table C1 shows that the length-scales are quite similar, stating that all variables have similar dominant spatial scales. The zero-crossing parameters of the three variables differ by only 25% while the spatial decay parameters are of the same order, even though the spatial decay for DIP is double than that of phytoplankton.

[91] The confidence levels of the field estimation are also estimated. The error variance in $\psi_{OA,x}$ is

$$VAR(\Psi_{OA,x}) = C_{x,x} - \sum_{q=1}^{N} C_{x,q} \cdot \left(\sum_{s=1}^{N} CC_{q,s}^{-1} \cdot C_{x,s}\right) \quad (\text{C3})$$

where $C_{x,x}$ is the covariance over the whole domain (natural variability) and $C_{x,r}$ and $C_{x,s}$ are the correlations between the point x and the sampling locations.

References

ARPAV (2002), Report on environmental status of the rivers of the Regione Veneto for the year 2001, in *Italian: Rapporto Sullo Stato Ambientale dei Corpi Idrici Anno 2001*, ARPAV Reg. Agency for the Protect. of the Environ., Venice, Italy.

Artegiani, A., D. Bregant, E. Paschini, N. Pinardi, F. Raicich, and A. Russo (1997), The Adriatic Sea general circulation. Part II: Baroclinic circulation structure, *J. Phys. Oceanogr.*, 27, 1515–1532.

Auclair, F., P. Marsaleix, and P. De Mey (2003), Space-Time structure and dynamics of the forecast error in a coastal circulation model of the Gulf of Lions, *Dyn. Atmos. Oceans*, 36, 309–346, doi:10.1016/S0377-0265(02)00068-4.

Bandelj, V., G. Socal, Y. Park, S. Lek, J. Coppola, E. Camatti, E. Capuzzo, L. Milani, and C. Solidoro (2008), Analysis of multitrophic plankton assemblages in the Lagoon of Venice, *Mar. Ecol. Prog. Ser.*, 368, 23–40, doi:10.3354/meps07565.

Bennett, A. F. (1992), Inverse methods in physical oceanography, in *Cambridge Monographs on Mechanics and Applied Mathematics*, Cambridge Univ. Press, Cambridge, U.K.

Bergamasco, A., and C. Zago (1999), Exploring the nitrogen cycle and macroalgae dynamics in the Lagoon of Venice using a multibox model, *Estuarine Coastal Shelf Sci.*, 48, 155–175.

Berline, L., J. M. Brankart, P. Brasseur, and J. Verron (2007), Improving the physics of a coupled physical-biogeochemical model of the North Atlantic through data assimilation: Impact on the ecosystem, *J. Mar. Syst.*, 64(1–4), 153–172.

Beşiktepe, T. S., P. F. J. Lermusiaux, and A. R. Robinson (2003), Coupled physical and biogeochemical data-driven simulations of Massachusetts Bay in late summer: Real-time and postcruise data assimilation, *J. Mar. Syst.*, 40–41, 171–212.

Bianchi, F., E. Ravagnan, F. Acri, F. Bernardi-Aubry, A. Boldrin, E. Camatti, D. Cassin, and M. Turchetto (2004), Variability and fluxes of hydrology, nutrients and particulate matter between the Venice Lagoon and the Adriatic Sea, preliminary results (years 2001–2002), *J. Mar. Syst.*, 51, 49–64.

Botter, G., T. Settin, M. Marani, and A. Rinaldo (2006), A stochastic model of nitrate transport and cycling at basin scale, *Water Resour. Res.*, 42, W04415, doi:10.1029/2005WR004599.

Bretherton, P. F., E. R. Davis, and C. B. Fandry (1976), A technique for objective analysis and design of oceanographic experiments applied to MODE-73, *Deep Sea Res.*, 23, 559–582.

Chiles, J.-P., and P. Delfiner (1999), *Geostatistics: Modeling Spatial Uncertainty*, Wiley, New York.

Ciavatta, S., R. Pastres, Z. Lin, M. B. Beck, C. Badetti, and G. Ferrari (2004), Fault detection in a real-time monitoring network for water quality in the Lagoon of Venice (Italy), *Water Sci. Technol.*, 11(50), 51–58.

Cloern, J. E. (2001), Our evolving conceptual model of the coastal eutrophication problem, *Mar. Ecol. Progr. Ser.*, 210, 223–253.

Cloern, J. E., and R. Dufford (2005), Phytoplankton community ecology: Principles applied in San Francisco Bay, *Mar. Ecol. Progr. Ser.*, 285, 11–28.

Cloern, J., C. Grenz, and L. Vidergar-Lucas (1995), An empirical model of the phytoplankton chlorophyll:carbon ration—The conversion factor between productivity and growth rate, *Limnol. Oceanogr.*, 40(7), 1313–1321.

Collavini, F., C. Bettiol, L. Zaggia, and R. Zonta (2005), Pollutant loads from the drainage basin to the Venice Lagoon (Italy), *Environ. Int.*, 31, 939–947.

Cossarini, G., S. Salon, S. Libralato, X. Gao, F. Giorgi, and C. Solidoro (2008), A downscaling experiment for the lagoon of Venice. Part II: Testing potential impacts of changes in precipitation temporal patterns on biogeochemical properties, *Clim. Res.*, 38(1), 43–59.

Cucco, A., and G. Umgiesser (2006), Modeling the Venice Lagoon residence time, *Ecol. Modell.*, 193(1–2), 34–51.

Curiel, D., A. Rismondo, G. Bellemo, and M. Marzocchi (2004), Macroalgal biomass and species variations in the Lagoon of Venice (Northern Adriatic Sea, Italy): 1981–1998, *Sci. Mar.*, 68(1), 57–67.

Dejak, C., D. Franco, R. Pastres, G. Pecenik, and C. Solidoro (1992), Thermal exchanges at air-water interfaces and reproduction of temperature vertical profiles in water columns, *J. Mar. Syst.*, 3, 465–476.

Dejak, C., R. Pastres, I. Polenghi, C. Solidoro, and G. Pecenik (1998), 3D modelling of water quality transport processes with time and space varying diffusivity, *Coastal Estuarine Stud.*, 54, 645–662.

Dickey, T. D. (2003), Emerging ocean observations for interdisciplinary data assimilation systems, *J. Mar. Syst.*, 40, 5–48.

Eknes, M., and G. Evensen (2002), An Ensemble Kalman filter with a 1-D marine ecosystem model, *J. Mar. Syst.*, 36(1–2), 75–100.

European Union (1996), Council directive 96/61/EC of 24 September 1996 concerning integrated pollution prevention and control, *Off. J. Eur. Communities*, 257, 0026–0040.

Facca, C., A. Sfriso, and G. Socal (2002), Changes in abundance and composition of phytoplankton and microphytobenthos due to increased sediment fluxes in the Venice Lagoon, Italy, *Estuarine, Coastal Shelf Sci.*, 54(5), 773–792, doi:10.1006/ecss.2001.0848.

Faugeras, B., O. Bernard, A. Sciandra, and M. Levy (2004), A mechanistic modelling and data assimilation approach to estimate the carbon/chlorophyll and carbon/nitrogen ratios in a coupled hydrodynamical-biological model, *Nonlinear Processes Geophys.*, 11(4), 515–533.

Friedrichs, M. A. M. (2001), A data assimilative marine ecosystem model of the central equatorial Pacific: Numerical twin experiments, *J. Mar. Res.*, 59, 859–894.

Friedrichs, M. A. M. (2002), Assimilation of JGOFS EqPac and SeaWiFS data into a marine ecosystem model of the central equatorial Pacific Ocean, *Deep Sea Res. Part II*, 49(1–3), 289–319.

Friedrichs, M. A. M., et al. (2007), Assessment of skill and portability in regional marine biogeochemical models: Role of multiple planktonic groups, *J. Geophys. Res.*, 112, C08001, doi:10.1029/2006JC003852.

Gačić, M., V. Kovačević, I. Mancero Mosquera, A. Mazzoldi, and S. Cosoli (2005), Water fluxes between the Venice Lagoon and the Adriatic Sea, in *Flooding and Environmental Challenges for Venice and Its Lagoon: State of Knowledge*, edited by C. A. Fletcher and D. T. Spencer, pp. 431–444, Cambridge Univ., Cambridge, U.K.

Garcia-Gorriz, E., N. Hoepffner, and M. Ouberdous (2003), Assimilation of SeaWiFS data in a couplet physical-biological model of the Adriatic Sea, *J. Mar. Syst.*, 40–41, 233–252.

Global Ocean Ecosystem Dynamics (GLOBEC) (2000), GLOBEC workshop: On the assimilation of biological data, in *Coupled Physical/Ecosystem Models*, edited by A. R. Robinson and P. F. J. Lermusiaux, CNR Research Area, Bologna, Italy.

Gregoire, M., P. Brasseur, and P. F. J. Lermusiaux (2003), Preface—33rd International Liege Colloquium on Ocean Dynamics—Liege, Belgium, May 7–11, 2001—The use of data assimilation in coupled hydrodynamic, ecological and biogeochemical models of the ocean, *J. Mar. Syst.*, 40, 1–3.

Guerzoni, S., P. Rossini, E. Molinaroli, G. Rampazzo, A. De Lazzari, and A. Zancanaro (2005a), Atmospheric bulk deposition to the Venice Lagoon: Part I. Fluxes of metals, nutrients and organic contaminants, *Environ. Int.*, 31, 959–974.

Guerzoni, S., G. Rampazzo, E. Molinaroli, and P. Rossini (2005b), Atmospheric bulk deposition to the Venice Lagoon: Part II. A source apportionment analysis in the vicinity of the industrial district of Porto Marghera, Italy, *Environ. Int.*, 31(7), 975–982.

Hemmings, J. C. P., M. A. Srokosz, P. Challenor, and R. Fasham (2003), Assimilating satellite ocean-colour observations into oceanic ecosystem models, *Philos. Trans. R. Soc. London*, 361(1802), 33–39.

Hofmann, E. E., and M. A. M. Friedrichs (2002), Predictive modeling for marine ecosystems, in *The Sea*, vol. 12, *Biological-Physical Interactions in the Ocean*, edited by A. R. Robinson, J. J. McCarthy, and B. J. Rothschild, pp. 537–565, John Wiley, New York.

Hofmann, E. E., and C. M. Lascara (1998), Overview of interdisciplinary modeling for marine ecosystems, in *The Sea*, vol. 10, *The Global Coastal Ocean: Processes and Methods*, edited by K. H. Brink and A. R. Robinson, pp. 507–541, Wiley, New York.

Holling, C. S. (1965), The functional response of predators to prey density and its role in mimicry and population regulation, *Mem. Entomological Soc. Can.*, 45, 1–60.

Hoteit, I., G. Triantafyllou, and G. Petihakis (2004), Towards a data assimilation system for the Cretan Sea ecosystem using a simplified Kalman filter, *J. Mar. Syst.*, 45(3–4), 159–171.

Hoteit, I., G. Triantafyllou, and G. Petihakis (2005), Efficient data assimilation into a complex, 3-D physical-biogeochemical model using partially-local Kalman filters, *Ann. Geophys.*, 23(10), 3171–3185.

IRSA570.1-Q59 (1990), Method n. 570.1, in *Metodi di Analisi per Acque di Mare, Quaderno No. 59*, Ist. Poligrafico e Zecca dello Stato Ed., Rome.

IRSA4010A-Q100 (1994), Method n. 4010A, in *Metodi Analitici per le Acque, Quaderno No. 100*, Ist. Poligrafico e Zecca dello Stato Ed., Rome.

Lasserre, P., and A. Marzollo (2000), *The Venice Lagoon Ecosystem: Inputs and Interactions Between Land and Sea (Man & the Biosphere)*, 533 pp., Taylor & Francis Ltd., Parthenon Group Inc., New York.

Lassiter, R. R., and D. K. Kearns (1974), Phytoplankton population changes and nutrient fluctuations in a simple aquatic ecosystem model, in *Modelling and Eutrophication Process*, edited by E. J. Middlebrookers, pp. 131–188, Ann Arbour Science, Ann Arbor, Mich.

Lermusiaux, P. F. J. (1999a), Data assimilation via error subspace statistical estimation. Part II: Middle Atlantic Bight shelfbreak front simulations and ESSE validation, *Mon. Weather Rev.*, 127, 1406–1432.

Lermusiaux, P. F. J. (1999b), Estimation and study of mesoscale variability in the Strait of Sicily, *Dyn. Atmos. Oceans*, 29, 255–303.

Lermusiaux, P. F. J. (2001), Evolving the subspace of the three-dimensional multiscale ocean variability: Massachusetts Bay, in *Special Issue on "Three-Dimensional Ocean Circulation: Lagrangian Measurements and Diagnostic Analyses"*, *J. Mar. Syst.*, vol. 29/1–4, pp. 385–422.

Lermusiaux, P. F. J. (2002), On the mapping of multivariate geophysical fields: Sensitivity to size, scales and dynamics, *J. Atmos. Ocean. Technol.*, 19, 1602–1637.

Lermusiaux, P. F. J. (2006), Uncertainty estimation and prediction for interdisciplinary ocean dynamics, *J. Comput. Phys.*, 217, 176–199.

Lermusiaux, P. F. J. (2007), Adaptive modeling, adaptive data assimilation and adaptive sampling, in *Special Issue on "Mathematical Issues and Challenges in Data Assimilation for Geophysical Systems: Interdisciplinary Perspectives"*, Phys. D, vol. 230, edited by C. K. R. T. Jones and K. Ide, pp. 172–196, Elsevier.

Lermusiaux, P. F. J., and A. R. Robinson (1999), Data assimilation via error subspace statistical estimation. Part I: Theory and schemes, *Mon. Weather Rev.*, 127, 1385–1406.

Lermusiaux, P. F. J., D. G. M. Anderson, and C. J. Lozano (2000), On the mapping of multivariate geophysical fields: Error and variability subspace estimates, *Q. J. R. Meteorol. Soc.*, April B, 1387–1430.

Lermusiaux, P. F. J., A. R. Robinson, P. J. Haley, and W. G. Leslie (2002), Advanced interdisciplinary data assimilation: Filtering and smoothing via error subspace statistical estimation, in *Proceedings of the OCEANS 2002 MTS/IEEE Conference*, pp. 795–802, Holland Publ.

Lermusiaux, P. F. J., C. Evangelinos, R. Tian, P. J. Haley, J. J. McCarthy, N. M. Patrikalakis, A. R. Robinson, and H. Schmidt (2004), Adaptive coupled physical and biogeochemical ocean predictions: A conceptual basis, *Lecture Notes Comput. Sci.*, 3038, 685–692.

Lermusiaux, P. F. J., P. Malanotte-Rizzoli, D. Stammer, J. Carton, J. Cummings, and A. M. Moore (2006a), Progress and prospects of U.S. data assimilation in ocean research, in *Oceanography. Special Issue on "Advances in Computational Oceanography"*, vol. 19, 1, edited by T. Paluszkiewicz and S. Harper, pp. 172–183, The Oceanography Society, Rockville, Md.

Lermusiaux, P. F. J., et al. (2006b), Quantifying uncertainties in ocean predictions, in *Oceanography. Special Issue on "Advances in Computational Oceanography"*, vol. 19, 1, edited by T. Paluszkiewicz and S. Harper, pp. 92–105.

Lermusiaux, P. F. J., P. J. Haley Jr., and N. K. Yilmaz (2007), Environmental prediction, path planning and adaptive sampling: Sensing and modeling for efficient ocean monitoring, management and pollution control, *Sea Technol.*, 48(9), 35–38.

Logutov, O. G. (2007), Multi-model fusion and uncertainty estimation for ocean prediction, Ph.D. dissertation, Harvard Univ, Cambridge, Mass.

Logutov, O. G., and P. F. J. Lermusiaux (2008), Inverse barotropic tidal estimation for regional ocean applications, *Ocean Modell.*, 25(1–2), 17–34, doi:10.1016/j.ocemod.2008.06.004.

Losa, S. N., G. A. Kivman, J. Schroter, and M. Wenzel (2003), Sequential weak constraint parameter estimation in an ecosystem model, *J. Mar. Syst.*, 43(1–2), 31–49.

Losa, S. N., G. A. Kivman, and V. A. Ryabchenko (2004), Weak constraint parameter estimation for a simple ocean ecosystem model: What can we learn about the model and data?, *J. Mar. Syst.*, 45(1–2), 1–20.

Lynch, R. D., and D. J. McGilicuddy Jr. (2001), Objective analysis for coastal regimes, *Cont. Shelf Res.*, 21, 1299–1315.

Magri, S., P. Brasseur, and G. Lacroix (2005), Data assimilation in a marine ecosystem model of the Ligurian Sea, *C. R. Geosci.*, 337(12), 1065–1074.

Malanotte-Rizzoli, P. (1996), *Modern Approaches to Data Assimilation in Ocean Modeling*, Elsevier Oceanogr. Ser., Elsevier Science B.V., Amsterdam, Netherlands.

MAV (2000), Report on the pollutant discharges from the P.Marghera industrial area for the year 1999, in *Italian Relazione Sulle Caratteristiche Degli Scarichi Idrici dell'Area di Porto Marghera. Dati Relativi al 1999*, 112 pp., Magistrato alle Acque di Venezia, Venice, Italy.

MAV (2002), Report on the pollutant discharges from the P.Marghera industrial area for the year 2000, in *Italian Relazione Sulle Caratteristiche Degli Scarichi Idrici dell'Area di Porto Marghera. Dati Relativi al 1999*, 142 pp., Magistrato alle Acque di Venezia, Venice, Italy.

Melaku Canu, D., G. Umgiesser, and C. Solidoro (2001), Short-term simulations under winter conditions in the Lagoon of Venice: A contribution to the environmental impact assessment of temporary closure of the inlets, *Ecol. Modell.*, 138(1–3), 215–230.

Michaelis, L., and M. Menten (1913), Die kinetik der invertinwirkung, *Biochem. Z.*, 49, 333–369.

Ministero dell'Ambiente (1999), Decreto ministeriale del 09/02/99. Carichi massimi ammissibili complessivi di inquinanti nella laguna di Venezia, *Gazzetta Uffic. Ital.*, 35, Rome, Italy.

Natvik, L.-J., and G. Evensen (2003), Assimilation of ocean colour data into a biochemical model of the North Atlantic. Part I: Data assimilation experiments, *J. Mar. Syst.*, 40–41, 127–153.

Oddo, P., N. Pinardi, M. Zavatarelli, and A. Coluccelli (2006), The Adriatic Basin forecasting system, *Acta Adriatica*, 47(Suppl.), 169–184.

Pastres, R., C. Solidoro, G. Cossarini, D. Melaku Canu, and C. Dejak (2001), Managing the rearing of *Tapes philippinarum* in the Lagoon of Venice: A decision support system, *Ecol. Modell.*, 138, 231–245.

Pastres, R., S. Ciavatta, G. Cossarini, and C. Solidoro (2003), Sensitivity analysis as a tool for the implementation of a water quality regulation based on the Maximum Permissible Loads policy, *Reliab. Eng. Syst. Safety*, 79, 239–244.

Pastres, R., C. Solidoro, S. Ciavatta, A. Petrizzo, and G. Cossarini (2004), Long-term changes of inorganic nutrients in the Lagoon of Venice (Italy), *J. Mar. Syst.*, 51, 179–189.

Pastres, R., S. Ciavatta, G. Cossarini, and C. Solidoro (2005), The seasonal distribution of dissolved inorganic nitrogen and phosphorous in the Lagoon of Venice: A numerical analysis, *Environ Int.*, 31, 1031–1039.

Press, W. H., S. A. Teukolsky, W. T. Vetterling, and B. P. Flannery (1992), *Numerical Recipes in Fortran 77: The Art of Scientific Computing*, Cambridge Univ. Press, Cambridge, U. K.

Pinardi, N., F. Auclair, C. Cesarini, E. Demirov, S. Fonda-Umani, M. Giani, G. Montanari, P. Oddo, M. Tonaniand, and M. Zavatarelli (2002), Towards marine environmental predictions in the Mediterranean Sea coastal areas: The Adriatic Sea example, in *Ocean Forecasting: Conceptual Basis and Applications*, edited by N. Pinardi and J. W. Woods, pp. 339–373, Springer and Verlag, Berlin, Germany.

Pinardi, N., G. Coppini, A. Grezio, and P. Oddo (2005), Ocean climate variability in the Mediterranean Sea: Climate events and marine forecasting activities, in *Flooding and Environmental Challenges for Venice and Its Lagoon: State of Knowledge*, edited by C. A. Fletcher and D. T. Spencer, Cambridge Univ. Press, Cambridge, U.K.

Raick, C., A. Alvera-Azcarate, A. Barth, J. M. Brankart, K. Soetaert, and M. Grégoire (2007), Application of a SEEK filter to a 1D biogeochemical model of the Ligurian Sea: Twin experiments and real in-situ data assimilation, *J. Mar. Syst.*, 65(1–4), 561–583.

Ridgwell, A., J. C. Hargreaves, N. R. Edwards, J. D. Annan, T. M. Lenton, R. Marsh, A. Yool, and A. Watson (2007), Marine geochemical data assimilation in an efficient Earth System Model of global biogeochemical cycling, *Biogeosciences*, 4(1), 87–104.

Rinaldo, A., G. Botter, E. Bertuzzo, A. Uccelli, T. Settin, and M. Marani (2006), Transport at basin scales: 2. Applications, *Hydrol. Earth Syst. Sci.*, 10, 31–48.

Rixen, M., E. Ferreira Coelho, and R. Signell (2008), Surface drift prediction in the Adriatic using hyper-ensembles statistics on atmospheric, ocean and wave models: Uncertainties and probability distribution areas, *J. Mar. Syst.*, 69, 86–98.

Robinson, A. R., and P. F. J. Lermusiaux (2001), Data assimilation in models, in *Encyclopedia of Ocean Sciences*, pp. 623–634, Acad. Press Ltd., London, U. K.

Robinson, A. R., and P. F. J. Lermusiaux (2002), Data assimilation for modeling and predicting coupled physical-biological interactions in the sea, in *The Sea*, vol. 12, *Biological-Physical Interactions in the Ocean*, edited by A. R. Robinson et al., pp. 475–536, Wiley, New York.

Robinson, A. R., P. F. J. Lermusiaux, and N. Q. Sloan (1998), Data assimilation, in *The Sea*, vol. 10, *The Global Coastal Ocean: Processes and Methods*, edited by K. H. Brink and A. R. Robinson, pp. 541–594, John Wiley, New York.

SAMA (2003), Report on water quality status and pollutant discharges from the P.Marghera industrial area for years 2001–2002, in *Italian: Qualità Delle Acque e Degli Scarichi Idrici dell'Area di Porto Marghera, Dati Relativi al 2001–2002*, Sezione Antinquinamento del Magistrato alle Acque, Venice, Italy.

Scavia, D., J. C. Field, and F. D. Boesch (2003), Forecasting climate impacts on coastal ecosystems, in *Ecological Forecasting: New Tools for Coastal and Ecosystem Management*, edited by N. J. Valette-Silver and D. Scavia, NOAA Technical Memorandum NOS NCCOS.

Sfriso, A., A. Marcomini, and B. Pavoni (1994), Annual nutrient exchanges between the central Lagoon of Venice and the northern Adriatic Sea, *Sci. Total Environ.*, 156, 77–92.

Sin, Y., and R. L. Wetzel (2002), Ecosystem modeling analysis of size structured phytoplankton dynamics in the York River estuary, Virginia (USA). I. Development of a plankton ecosystem model with explicit feedback controls and hydrodynamics, *Mar. Ecol. Progr. Ser.*, 228, 75–90.

Socal, G., F. Bianchi, and L. Alberighi (1999), Effects of thermal pollution and nutrient discharges on a spring phytoplankton bloom in the industrial area of the Lagoon of Venice, *Vie Milieu*, 49(1), 19–31.

Solidoro, C., A. Crise, G. Crispi, and R. Pastres (2003), An a priori approach to assimilation of ecological data in marine ecosystem models, *J. Mar. Syst.*, 40, 79–97.

Solidoro, C., R. Pastres, G. Cossarini, and S. Ciavatta (2004), Seasonal and spatial variability of water quality parameters in the Lagoon of Venice, *J. Mar. Syst.*, 51, 7–18.

Solidoro, C., R. Pastres, and G. Cossarini (2005a), Nitrogen and plankton dynamics in the Lagoon of Venice, *Ecol. Modell.*, 184, 103–124.

Solidoro, C., R. Pastres, and D. Melaku Canu (2005b), Modelling water quality and ecological processes in the Lagoon of Venice: A review, in *Flooding and Environmental Challenges for Venice and Its Lagoon: State of Knowledge*, edited by C. A. Fletcher and T. Spencer, pp. 529–545, Cambridge Univ. Press, Cambridge, U.K.

Solidoro, C., R. Pastres, G. Cossarini, D. Melaku Canu, and S. Ciavatta (2006), Order and chaos in the natural world, in Exploring and understanding variability in the lagoon of Venice, *Int. J. Ecodyn.*, 1(4), 1–9.

Spitz, Y. H., J. R. Moisan, and M. R. Abbott (2001), Configuring an ecosystem model using data from the Bermuda Atlantic Time Series (BATS), *Deep Sea Res. Part II*, 48(8–9), 1733–1768.

Steele, J. H. (1962), Environmental control of photosynthesis in the sea, *Limnol. Oceanogr.*, 7, 137–150.

Strickland, J. D., and T. R. Parsons (1972), A practical handbook of seawater analysis, *Bull. Fish. Res. Board Can.*, 167, Fisheries Research Board of Canada, Halifax, Canada.

Suman, D., S. Guerzoni, and E. Molinaroli (2005), Integrated coastal management in the Venice lagoon and its watershed, *Hydrobiologia*, 550, 251–269.

Testa, J. M., W. M. Kemp, W. R. Boynton, and J. D. Hagy (2008), Long-term change in water quality and productivity in the Patuxent River Estuary: 1985 To 2003, *Estuaries Coasts*, 31, 1021–1037.

Tian, R. C., P. F. J. Lermusiaux, J. J. McCarthy, and A. R. Robinson (2004), A generalized prognostic model of marine biogeochemical-ecosystem dynamics: Structure, parameterization and adaptive modeling. May 2004, *Harvard Rep. Phys./Interdisciplinary Ocean Sci.*, 67, 1–65.

Tjiputra, J. F., D. Polzin, and A. M. E. Winguth (2007), Assimilation of seasonal chlorophyll and nutrient data into an adjoint three-dimensional ocean carbon cycle model: Sensitivity analysis and ecosystem parameter optimization, *Global Biogeochem. Cycles*, 21(1), GB1001, doi:10.1029/2006GB002745.

Triantafyllou, G., I. Hoteit, and G. Petihakis (2003), A singular evolutive interpolated Kalman filter for efficient data assimilation in a 3-D complex physical-biogeochemical model of the Cretan Sea, *J. Mar. Syst.*, 40–41, 213–231.

Triantafyllou, G., G. Korres, I. Hoteit, G. Petihakis, and A. C. Banks (2007), Assimilation of ocean colour data into a biogeochemical flux model of the eastern Mediterranean Sea, *Ocean Sci.*, 3(3), 397–410.

Wang, D., P. F. J. Lermusiaux, P. J. Haley, D. Eickstedt, W. G. Leslie, and H. Schmidt (2009), Acoustically focused adaptive sampling and on-board routing for marine rapid environmental assessment, in *Special Issue on "MREA and Coastal Processes: Challenges for Monitoring and Prediction"*, edited by J. W. Book, M. Orlic, and M. Rixen (Guest Eds.), *J. Mar. Sys.*, doi:10.1016/j.jmarsys.2009.01.037.

Wunsch, C. (1996), *The Ocean Circulation Inverse Problem*, Cambridge Univ. Press, New York.

Yilmaz, N. K., C. Evangelinos, P. F. J. Lermusiaux, and N. Patrikalakis (2008), Path planning of autonomous underwater vehicles for adaptive sampling using mixed integer linear programming, *IEEE Ocean Eng.*, 33(4), 522–537, doi:10.1109/joe.2008.2002105.

Zirino, A. (2005), The monitoring programme in the Venice Lagoon: Striving towards a comprehensive knowledge of the Lagoon ecosystem, in *Flooding and Environmental Challenges for Venice and Its Lagoon: State of Knowledge*, edited by C. A. Fletcher and T. Spencer, pp. 505–516, Cambridge Univ. Press, Cambridge, U.K.

Zonta, R., F. Costa, F. Collavini, and L. Zaggia (2005), Objectives and structure of the DRAIN project: An extensive study of the delivery from the drainage basin of the Venice Lagoon (Italy), *Environ. Int.*, 31, 923–928.

Zuliani, A., L. Zaggia, F. Collavini, and R. Zonta (2005), Freshwater discharge from the drainage basin to the Venice Lagoon (Italy), *Environ. Int.*, 31, 929–938.

————————————

G. Cossarini and C. Solidoro, Department of Oceanography, Istituto Nazionale di Oceanografia e di Geofisica Sperimentale, Borgo Grotta Gigante, 42/c, 34010, Sgonico (TS), Italy. (gcossarini@ogs.trieste.it)

P. F. J. Lermusiaux, Department of Mechanical Engineering, Massachusetts Institute of Technology, 77 Massachusetts Avenue, Cambridge, MA 02139-43071, USA. (pierrel@mit.edu)